Topography-driven hydrothermal breccia mineralization of Pliocene age at Grimsel Paa, Aar massif, Central Swiss Alps

Autor(en): **Hofmann, Beda A. / Helfer, Michael / Diamond, Larryn W.**

Objekttyp: **Article**

Zeitschrift: **Schweizerische mineralogische und petrographische Mitteilungen = Bulletin suisse de minéralogie et pétrographie**

Band (Jahr): **84 (2004)**

Heft 3

PDF erstellt am: **24.04.2024**

Persistenter Link: https://doi.org/10.5169/seals-63750

Schweizerische Mineralogische und Petrographische Mitteilungen 84, 271–302, 2004

Topography-driven hydrothermal breccia mineralization of Pliocene age at Grimsel Pass, Aar massif, Central Swiss Alps

Beda A. Hofmann[1], *Michael Helfer*[1*], *Larryn W. Diamond*[2], *Igor M. Villa*[3], *Robert Frei*[3**] and *Jost Eikenberg*[4]

Abstract

Fault-bound hydrothermally mineralized breccias with a multistage deformation history occur in crystalline rocks of the Aar massif at Grimsel Pass, Central Swiss Alps. The breccias crop out over 4.5 km E–W along strike and over 900 m in vertical extent between Trübtensee and Gletsch, and are up to 2 m wide. A characterization of these "Grimsel Breccias" was carried out to elucidate their formation with respect to alpine uplift and fluid circulation history, and to search for possible evidence of past microbial activity.

Breccias vary widely in grain size and range from matrix-rich to clast-supported with high porosity in the youngest equivalents. Centimeter-sized voids typically contain stratified geopetal infills of fine-grained hydrothermal minerals. The hydrothermal mineral assemblage is dominated by quartz (including chalcedony), adularia, illite, celadonitic clay minerals, pyrite (As-rich), marcasite, and fine-grained Mo-sulfide. Analyses of bulk rocks (kg) and small subsamples (grams) show significant enrichments of Mo, As, Sb, Au, Cs, Hg, Tl and in some samples of U.

Subthermal to thermal springs are currently discharging from the breccia zone at Gletsch (18–19 °C) and into a gas pipeline tunnel intersecting the breccia (up to 28 °C), indicating ongoing deep fluid circulation in a fracture system related to the Grimsel Breccia. Microbial biomass and Fe–Mn precipitates from thermal springs are enriched in Au, Cs, Sb, Hg, Pb, Mn, W, demonstrating that several of the elements enriched in the breccia are also currently transported and/or redistributed in the active water circulation system.

$^{39}Ar/^{40}Ar$ dating of late-stage adularia yielded a middle Pliocene age (3.30±0.06 Ma), indicating formation between 0.3 and 1.2 km below sea level, if current uplift rates of the Aar massif are assumed. The estimated depth of formation is ~3 km below the palaeosurface. Oxygen isotopes in quartz and adularia, combined with fluid inclusion data, indicate a formation temperature ranging from 160 down to approximately 100 °C at the latest stage. Fluids were of low-salinity with a dominant meteoric component with $\delta^{18}O$ close to –10‰ SMOW. δD values of illite-rich samples are also consistent with formation from meteoric water. Pyrite $\delta^{34}S$ shows limited scatter with a slightly negative average of –1.8‰ CDT, consistent with an origin of the sulfide by thermochemical reduction of Triassic sulfate at 220–260 °C at greater depth.

A search for signatures of possible microbial activity during breccia formation revealed the presence of extremely fine-grained pyrite and uraninite of potential microbiological origin, some ill-preserved filamentous structures and laminated fabrics potentially related to biofilms, but no indisputable evidence of biological involvement.

The hydrothermal breccia mineralization in the Grimsel area demonstrates that meteoric waters penetrated deep into the Aar massif in the Pliocene and caused mineralizations geochemically similar to epithermal ores typically associated with volcanism. The enriched elements probably are derived from a combination of deep sources (Au, As, Sb, Tl) and near-surface oxidized fluids (Mo, U), and element precipitation may be a result of mixing and/or cooling.

Keywords: Hydrothermal breccia, Pliocene, Aar massif, molybdenum, arsenic, gold, thermal springs.

1. Introduction

Epithermal systems are important ore-forming environments where they are associated with magmatism (Jobson et al., 1994; Krupp and Seward, 1987; Sillitoe, 1993; Hedenquist and Lowenstern, 1994), but deposition of significant amounts of economically interesting elements from hydrothermal systems resulting from topography-driven deep water circulation in mountain belts apparently is uncommon.

Uplift and erosion of the Alps has long been recognized to be associated with mineral forming processes, most notably in Alpinotype fissures

[1] Naturhistorisches Museum Bern, Bernastrasse 15, CH-3005 Bern, Switzerland. <beda.hofmann@nmbe.unibe.ch>
[2] Institut für Geologie der Universität Bern, Baltzerstrasse 1-3, CH-3012 Bern, Switzerland.
[3] Institut für Geologie der Universität Bern, Erlachstrasse 9a, CH-3012 Bern, Switzerland.
[4] Paul Scherrer Institut, CH-5232 Villigen, Switzerland.
* Present address: Dorfbachstr. 76, Köniz, Switzerland.
** Present address: Geological Institute, University of Copenhagen, Copenhagen, Denmark.

0036-7699/04/0084/271

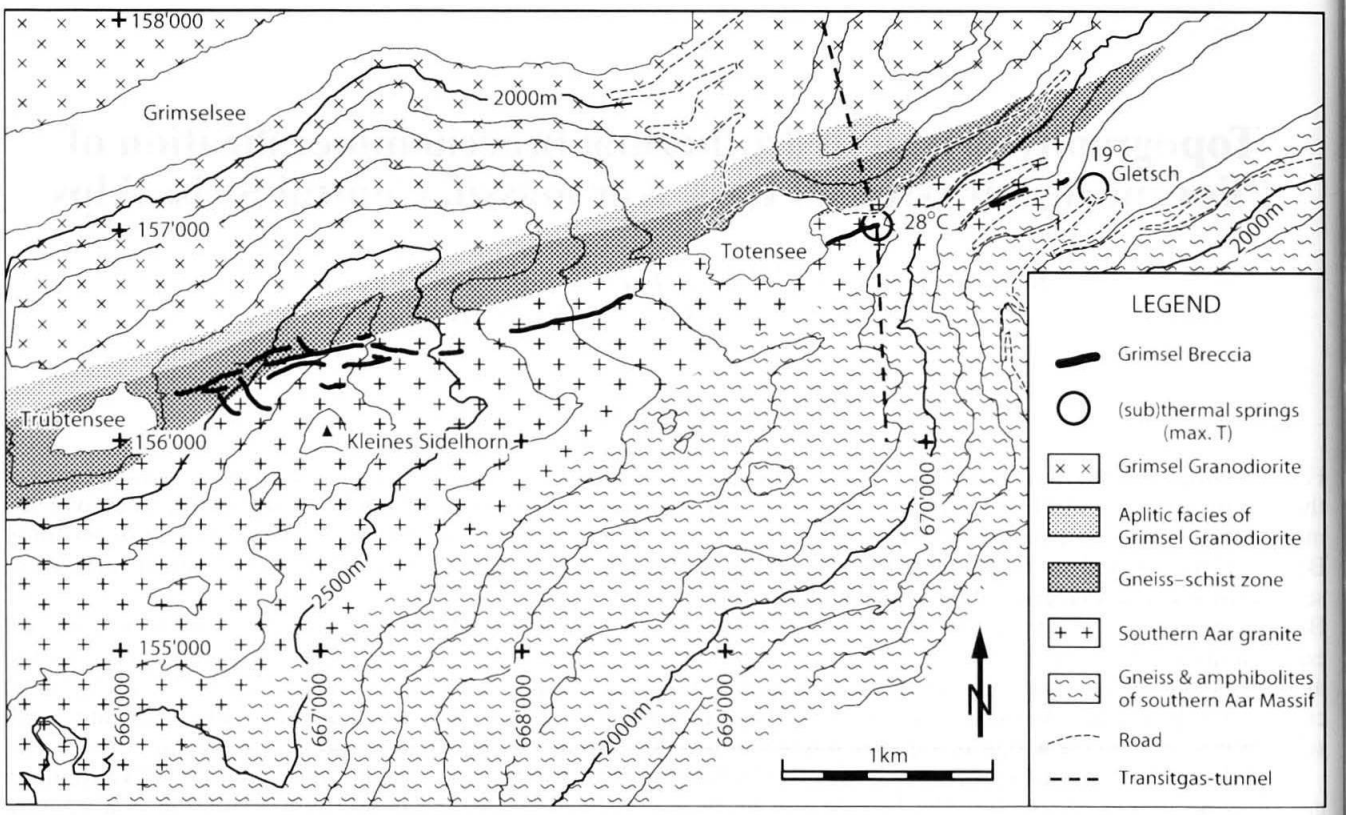

Fig. 1 Simplified geological map of the Grimsel pass area showing the extent of Grimsel Breccia outcrops and the location of related (sub)thermal springs. Geology mainly based on Stalder (1964) and Niggli (1965).

that were formed in a temperature range between 400 and 200 °C and depths of between 15 and 10 km (Mullis et al., 1994; Stalder, 1964). Mesothermal gold veins of Alpine age are common in the Penninic Alps, e.g. at Brusson, but their origin is related to fluids derived from much greater depth (Pettke and Diamond, 1997; Pettke et al., 1999, 2000). Other types of late Alpine mineralizations are less well known and comprise needle quartz veins, zeolite-rich assemblages in breccias at Gibelsbach, Valais (Armbruster et al., 1996) and collomorph fluorite at Kleines Furkahorn, Valais (Stalder et al., 1998).

The aim of this study was a characterization of hydrothermally influenced breccias between Gletsch and Kleines Sidelhorn, Grimsel area, Central Swiss Alps. These breccias were first described and mapped by Stalder (1964) and later by Dollinger (1989), but the total extent and the conditions of formation and the age were unknown. Uranium prospection in the 1970s revealed a small area of U-rich breccias (T. Labhart and J. Abrecht, pers. comm. 1996). Active thermal springs (Degueldre et al., 1989; Pfeifer et al., 1992) in the Transitgas tunnel 0.8 km E of the Grimsel Pass near the known occurrence of breccias and at Gletsch (Niggli, 1965) indicated possible ongoing hydrothermal activity. One of the main reasons for the initiation of the present characterization study was the possibility that the Grimsel Breccia represents a low-temperature hydrothermal system formerly colonized by microbes. This appeared a particularly interesting possibility because a study of the Carboniferous Menzenschwand hydrothermal veins in the Black Forest, Germany (Hofmann, 1989) indicated the possible presence of microbial fossils in a system exhibiting many petrographic similarities. Meanwhile many other localities have been investigated, some of which yield better evidence for the former presence of subsurface microbes than the Grimsel system (Hofmann and Farmer, 1997, 2000). This study revealed that the Grimsel Breccia is significantly enriched in Au and Mo and therefore documents a rare case of a young, mineralized hydrothermal system that, based on the regional absence of magmatic activity and the prevalence of meteoric water, was driven by topography.

The study of the Grimsel Breccia also appeared interesting in the light of regional late Alpine to recent tectonics. Indications of recent tectonic activity have been claimed to be present along the northern mountain slopes of the Rhone-Rhine Valley (Eckardt et al., 1983). However, evidence of recent seismicity in this zone is missing (Pavoni et al., 1997) and an interpretation of the apparent recent fault feature as a result of

near-surface mass wasting ("Hakenwurf") is possible (A. Steck, pers. comm. 1997). The Grimsel Breccia is situated in this zone of supposed young tectonic activity (Eckardt et al., 1983; Stalder, 1964) as are the Grimsel hydroelectric reservoirs. The age of this tectonic and hydrothermal activity is relevant, therefore, to the safety assessment of existing and possible future reservoirs.

2. Geological context and regional geology

The area under investigation is located in the southern part of the Aar massif, a paraautochthonous crystalline unit in the Central Swiss Alps measuring about 115 km in E–W and up to 23 km in N–S extent (Steck, 1968). Rocks are mainly gneisses and granites of Variscan and older age (Schaltegger and Corfu, 1992) with minor metasediments and metavolcanics, and have undergone greenschist metamorphism during the Alpine orogeny (Frey and Ferreiro Mählmann, 1999). The main geological units in the Grimsel Pass area are (from N to S, see Fig. 1) the Central Aar Granite (297±2 Ma, Schaltegger and Corfu, 1992), the Grimsel Granodiorite (299±2 Ma, Schaltegger and Corfu, 1992) with an aplitic border facies in the south, the Gneiss-schist zone with gneisses, micaschists, migmatites and amphibolites, the Southern Aar Granite (age approx. 350 Ma, Schaltegger and Corfu, 1992) and the Southern Border Zone with gneisses and schists (Niggli, 1965). Detailed geological investigations have been performed in the Nagra Rock Laboratory located just 2.5 km north of the most prominent breccia zone. No evidence of recent hydrothermal activity has been detected there (Keusen et al., 1989; Baertschi et al., 1991; Kralik et al., 1992). The late Alpine uplift history in the Grimsel area has been studied in some detail using radiometric age dating and fluid inclusion measurements (Michalski and Soom, 1990; Schaltegger and Corfu, 1992; Mullis et al., 1994). The present-day geothermal gradient is approximately 25°C/km (Bodmer, 1982), the rate of uplift approximately 0.9 mm/a (Kahle et al., 1997). The occurrence of a breccia cemented by chalcedony in the Gneiss-schist-zone south of Trübtensee was first observed by Stalder (1964) and also described by Dollinger (1989).

3. Samples and methods

Samples for this study were largely collected during field seasons 1995–1997, but we also investigated some samples collected during earlier studies (Stalder, 1964; Dollinger, 1989) and during uranium prospection activities in the 1970s. The investigated samples are deposited in the collections of the Natural History Museum in Bern. A short description and localities for all mentioned samples is given in Appendix 1.

The petrographic study is based on the investigation of rock slabs, thin- and polished sections supported by electron microprobe analysis and mineral identification by XRD.

For SEM observations, quartz-samples were cleaned with HCl to remove Fe-hydroxides and sodium hypochlorite to remove organics (lichen). Some samples were etched in 5% HF for 10–60 minutes.

Geochemical analyses were performed on bulk samples of homogenized and powdered breccias and host rocks applying a combination of INAA (instrumental neutron activation), ICP-OES (inductively-coupled plasma-optical emission spectrometry), AA (atomic absorption), FA-DCP (fire-assay-preconcentration-direct current plasma emission spectrometry) and ISE (ion selective electrode for fluoride) techniques. Chip samples averaging 0.2 to 1 g taken from well-defined petrographic units of breccias were analyzed without further preparation by INAA only. Analyses were performed by Bondar Clegg laboratories (Toronto) for bulk breccias and by Becquerel Laboratories (Mississauga, Ontario) for INAA on chips. In most cases for each sample two powders were analyzed, one prepared in a tungsten carbide and the other in a stainless steel mill. In this way results uncontaminated for both W/Co and Fe/Cr could be obtained. Recent spring deposits were collected in the Transitgas tunnel in areas of maximum discharge from the warmest springs. Soft precipitates were collected with syringes and brought into the laboratory as slurry in water. After decanting and filtering, the dried residues were ground and treated as the other rock powders.

Stable isotopes of O and S were measured at the Institut de Minéralogie et Pétrographie, Lausanne University, using methods desribed in Sharp (1990, 1992) and Valenza et al. (2000). Quartz samples were measured using laser fluorination of mm-sized chips. Sulfides were extracted by dissolution of breccia samples in HF followed by heavy liquid separation and/or micropanning. A second suite of sulfide samples as well as H isotope measurements were performed by Geochron Laboratories (Cambridge, MA, USA). Procedures for the applied U/Pb analytical methods are described in Hofmann and Frei (1996). The method applied for alphaspectroscopy included separation of radionuclides using the method described by Horwitz et al. (1992) followed by elec-

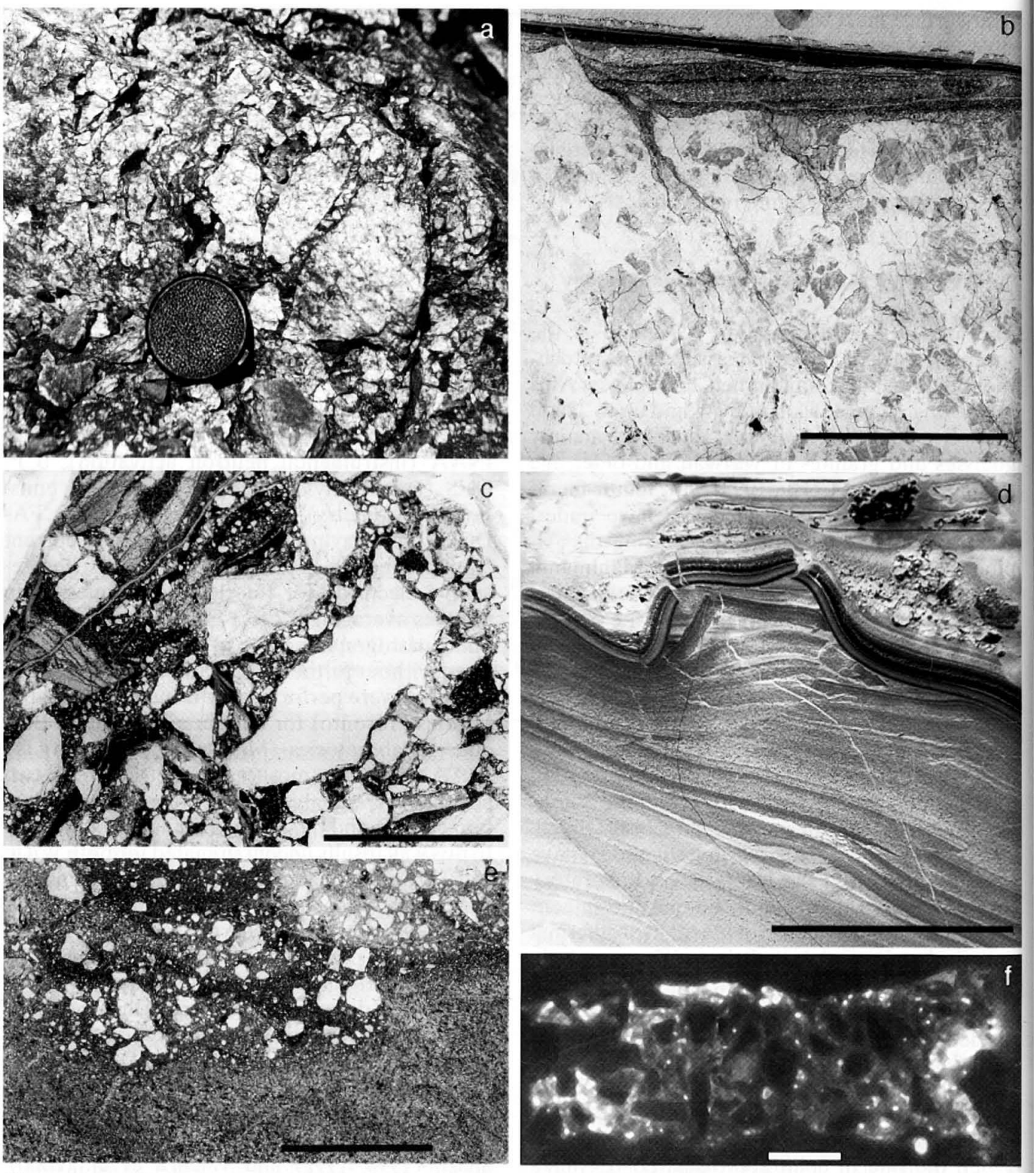

Fig. 2 Grimsel Breccia textures: (a) Typical breccia outcrop N of Kleines Sidelhorn. Lens cap diameter 6 cm; (b–e) examples of multistage breccias and geopetal infills, (b) fining-upward sediment on granite (GR7), (c) breccia with clasts of quartz-rich breccia (light, gulfed areas due to clast heterogeneity, not dissolution) and sediment clasts (GR28), (d) soft-sediment deformation (GR41), (e) irregular boundary (deformed?) between fine-grained, well-sorted sediment and breccia (GR26); (f) autoradiograph of uranium-rich breccia vein demonstrating uranium enrichment in the matrix (courtesy T. Labhart). Scale bars are 10 mm in all images.

trodeposition on stainless steel discs according to the procedure given by Bajo and Eikenberg (1999). Measurement of the planar sources was carried out by means of ion implanted surface barrier alpha detectors (system Octette, EG&G Ortec). ^{39}Ar–^{40}Ar-dating was performed by a routine described in detail in Belluso et al. (2000). Fluid inclusions were measured microthermometrically on double-polished sections using a Linkam THMSG 600 heating-freezing stage, cali-

brated against phase transitions in synthetic fluid inclusions. All measurements were made with a 100× objective lens.

4. Results

4.1. Field geology of the Grimsel Breccia

The Grimsel Breccia is a cataclastic fault zone a few decimeters to several meters wide, generally consisting of a single near vertical sheet-like breccia body. Fractures perpendicular to the main breccia body typically are filled with breccia and quartz/chalcedony as well and fan out into the surrounding rock. The breccia body is discontinous with a geometry consistent with a formation as infills of dilatational fault jogs along a strike-slip fault (Sibson, 1987). The general trend of the Grimsel Breccia is WSW–ENE from east of Trübtensee over the ridge east of the Sidelhorn, down to the Totensee and then towards Gletsch (Fig. 1), the average strike is 076°E and the dip is near vertical. The breccia cuts across the gneiss-schist-zone in the westernmost part, runs into the southern Aar granite and passes into the southern border zone NW of Gletsch. The easternmost outcrop is approximately 150 m west of the subthermal spring of Gletsch. We also observed the Grimsel Breccia in the Transitgas tunnel about 200 m east of the Totensee and 165 m below a surface breccia outcrop. Breccia outcrops were mapped over a total length of 4.4 km and a maximum vertical range of 900 m (1800–2700 m above sea level). On some late faults in the breccia slickensides were observed, their lineation showing consistent westward plunge of 15–43°.

Attempts to map the Grimsel Breccia on aerial photographs were not successful. Large numbers of photolineations coincide with the mapped breccia only at a few places. Most photolineations appear to be related to lithologic contacts and unmineralized faults and shear zones apparently unrelated to the breccia. Where it is silica-cemented, the breccia is very hard and resistant to weathering, forming small ridges. In contrast to most host rocks it typically shows a rusty stain. The Grimsel Breccia clearly is testimony of a polyphase breccia formation process. Early low porosity phases are reworked and cut by faults.

Close to the breccia, the wall rocks are strongly fractured. Coatings of black quartz/chalcedony on fractures are ubiquitous in its vicinity. The breccia is very heterogeneous ranging from fine-grained dense (low porosity) to varieties with large components. Often it shows little sorting with millimeter- and decimeter-sized fragments in contact. Geopetal infills in large pore spaces are common. Transitions between different breccia lithologies are often gradual, but in places matrix-rich fine-grained varieties may be in sharp contact with coarse porous types, with a boundary parallel to the general trend. Highly porous breccias were observed only in the upper part of the outcrops (>2000 m above sea level). Alpinotype fissures are sometimes intersected by the Grimsel Breccia, clearly showing the latter to have resulted from a much later event, with alpintotype quartz crystals being coated by fine-grained quartz/chalcedony.

A type of breccia rich in uranium is present in small outcrops N of Sidelhorn. These occurrences were discovered during uranium prospection around 1977 (pers. comm. T. Labhart, J. Abrecht, 1995) and could be relocated only in traces during this study. Samples collected during uranium prospection show petrographic and geochemical signatures closely resembling the other samples of Grimsel Breccia.

Our mapping showed a clear and previously unrecognized spatial association (Fig. 1) between the Grimsel Breccia and the (sub)thermal springs near Gletsch (Niggli, 1965) and in the Transitgas-tunnel (Pfeifer et al., 1992), where thermal water is discharging from a zone showing Grimsel Breccia characteristics such as chalcedony coatings. Water temperatures were 18.4–20.0 °C for Gletsch (July 1996 to November 1997) and up to 28.2 °C in the Transitgas tunnel (July 1998). This close association indicates that the Grimsel Breccia most likely is the main flow path for the present discharge of (sub)thermal waters.

4.2. Petrography of hydrothermal breccias

Detailed petrographic investigations of the Grimsel Breccia were used to construct a model suitable to explain all petrographic breccia varieties. Macroscopic and microscopic aspects of the Grimsel Breccia are shown in Figures 2 and 3. The breccia consists of three principal components:

I. Clasts consisting of host rock fragments or earlier breccia stages. Clasts are generally angular to subangular and range in size from ~10 cm to submicroscopic (Figs. 2, 3). In a few cases well-rounded quartz grains of sand-grain size were observed (Fig. 3d). Sorting is generally poor, but some breccia samples are well sorted mostly in the sand-to-silt grain size, with gradual transitions to geopetal infills. Clast petrography generally reflects the host rocks, indicating that no significant particle movement occurred.

II. Fine-grained siliceous chert, consisting of microcrystalline hydrothermal quartz, minor hy-

drothermal clays, and rock flour, occurring as breccia matrix, geopetal infills, fracture infill or mantling clasts (Figs. 2d,e, 3b,c). This chert contains variable amounts of clay minerals, rock fragments and sulfides. The color ranges from light gray to black.

III. Pore-filling cement consisting of the fibrous quartz varieties chalcedony (length-fast) and quartzine (length-slow, Stalder, 1964), megaquartz and minor adularia, sometimes interlayered with chert (Fig. 3b). A celadonitic clay mineral (always weathered in open pores) is present as very late stage cement.

Typical examples of breccia textures are shown in Fig. 2. Breccia types range from fractured but largely intact host rock to matrix-supported breccias including fine-grained fault gouges and clast-supported breccias with open porosity. Abundant macroporosity (up to 25% with pores exceeding 2 cm) is typical of the latest breccia stages at the higher elevations (>2000 m above sea level). Earlier breccias as well as samples from lower elevations near Gletsch are dense and free of macroporosity. Dense breccias sometimes contain clasts showing evidence of "pisolitic" or "lapilli-like" particle accretion ("pelletization") around clasts, and a few examples of "pellets" entirely consisting of fine-grained breccia were observed (Fig. 3e,f). Multiple brecciation events are evidenced by several generations of breccia clasts. Paragenetically older breccia clasts often show evidence of quartz recrystallization.

Finely stratified geopetal infills are very common in fractures and large pores between fragments. These sediments consist of chert with variable amounts of clay minerals and rock fragments, typically consisting of several subsequent fining-upwards cycles. Chert typically is interlayered with fine-grained quartz cement. Brecciation and soft-sediment deformation of geopetal infills is quite common (Fig. 2d). Individual sediment layers range in thickness from a few μm to several millimeters.

Sediment layering initially is absolutely horizontal in the case of geopetal sediments (Fig. 3c). In other cases, "sediment layers" following the contours of uneven substrates were observed, implying accretion by agglutination and not just sedimentation. We will refer to these as "banded chert/quartz" (BCQ). Facies changes from geopetal sediments to BCQ and vice versa can often be observed.

Host rocks often show a high degree of higher-temperature cataclastic to mylonitic deformation in the vicinity of the breccia, but entirely undeformed and unaltered host rocks in direct contact with the Grimsel Breccia can also be observed. Evidence of hydrothermal host rock alteration is notably absent even in direct contact with the breccia.

Breccias are significantly oxidized in outcrops. Black sulfidic breccias show up to 5 mm thick brown weathering zones indicative of sulfide oxidation. Sulfidic breccias and weathering rinds are often separated by a light zone devoid of both sulfides and Fe-hydroxides. However, weathering in breccias is often much less pervasive than in the host rock, probably due to the low permeability of silica-rich breccias.

4.3. Mineralogy and mineral chemistry

The relatively simple mineralogy of the Grimsel Breccia is characterized by only a few neoformed species: By far the dominant mineral is quartz, mainly in microcrystalline form. Celadonitic clay minerals and adularia are locally abundant. Only sparse fluorite has been observed. The Grimsel Breccia is absolutely devoid of carbonate minerals. Sulfides are common but restricted to pyrite, marcasite and microcrystalline molybdenite. Only very locally uranium-rich breccias containing fine-grained uraninite are developed.

Quartz varieties constitute by far the largest proportion of neoformed minerals in the Grimsel Breccia. Most of the quartz is microcrystalline, with chert-like varieties dominating as matrix in breccias. Quartz with a crystal size of 50–250 μm is the most common breccia cement, while fibrous chalcedony and quartzine occurs only rarely as thin (1 mm) crusts. Large (>1 mm) crystals of quartz occur sparingly as early precipitate and in some druses of uncertain paragenetic stage. Some druse quartz shows a pronounced rhombohedral (pseudocubic) habit, with only one set of rhombohedra developed. The presence of opal (Stalder et al., 1998) could not be confirmed during this study, all investigated samples showing well-crystallized quartz by X-ray diffractometry and birefringence in thin section, even though some samples are extremely fine-grained. This result is in agreement with a study of hydrothermal sinters by Herdianita et al. (2000), who found sinters >50'000 years in age to consist of microcrystalline quartz. The finest-grained cherts are olive-green due to their content of celadonitic clay minerals and occur 400 m W of Gletsch. Quartz paramorphs after a disc-shaped mineral were observed in some druses with quartz crystals.

The occurrence of phyllosilicates as neoformation in the Grimsel Breccia is of irregular distribution. Common colorless mica/illite in breccia matrices and sediments probably contains a detrital component. This mica/clay mineral is Fe-poor (no positive Fe–K correlation in 266 microprobe anal-

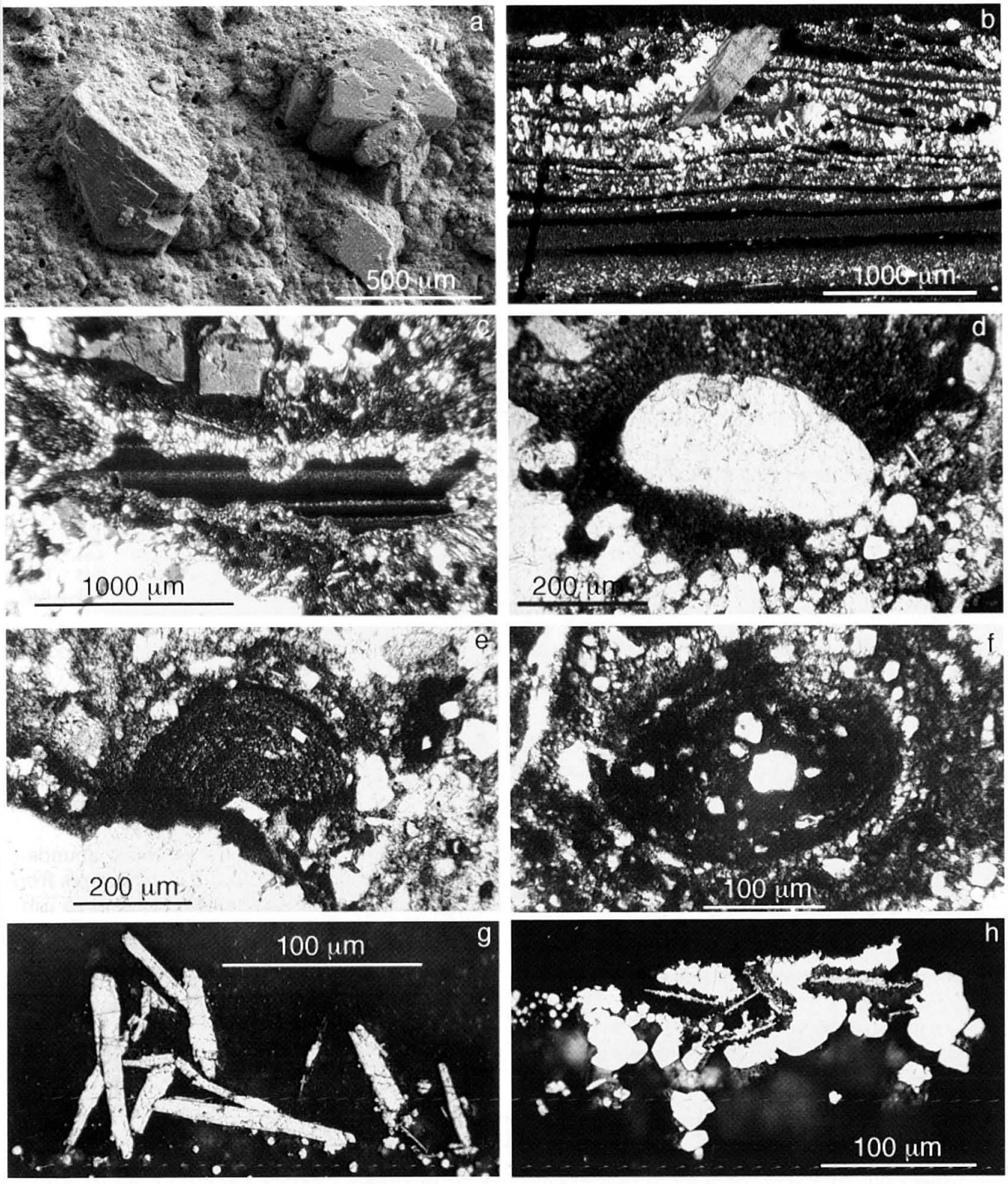

Fig. 3 Microscopic breccia features. (a) SEM-image showing euhedral adularia on late-stage surface, partially covered by fine-grained quartz-rich sediment (GR23); (b) laminated undulous quartz/sediment deposit with in-situ grown adularia, crossed polarizers (GR7); (c) geopetal infill of pore, crossed polarizers (GR1); (d) well-rounded polycrystalline quartz grain in breccia matrix, plane polarized light (GR28); (e, f) accretionary "pellets" consisting of mineral fragments in clay-rich matrix, plane polarized light (GR28, 52); (g, h) pseudomorphs of pyrite/marcasite after pyrrhotite?, associated with euhedral pyrite, reflected light, oil immersion (GR2).

yses of breccia matrix). A second type of phyllosilicate is most abundant in greenish breccias occurring 500 m west of Gletsch at about 1900 m altitude, but is also present in uranium-rich breccia matrices from some of the highest outcrops N of Sidelhorn, where it is also present as very late

Table 1 Microprobe data for celadonitic clay minerals, sample GR 84. Analyses arranged in order of decreasing Fe/(Fe+Al).

Analysis No.	7	22	6	23	8	4	17	21	16	13	29	20	19	28	MEAN
SiO_2	41.63	44.32	45.20	42.64	45.34	45.83	43.92	48.23	50.33	49.55	41.26	51.28	46.71	42.77	45.64
TiO_2	0.00	0.01	0.03	0.01	0.00	0.00	0.00	0.01	0.01	0.03	1.20	0.02	0.02	0.81	0.15
Al_2O_3	12.15	12.44	12.37	12.92	12.66	12.87	15.64	13.11	13.03	13.49	24.45	14.65	16.56	25.92	15.16
Fe_2O_3	17.60	15.72	15.56	14.75	14.53	14.25	14.95	12.02	12.50	10.60	9.75	6.65	6.27	6.08	12.23
FeO	9.10	9.05	9.12	8.82	9.10	9.19	9.83	8.45	11.20	10.60	6.12	8.46	8.97	7.60	8.97
MnO	0.10	0.05	0.17	0.10	0.09	0.10	0.07	0.15	0.03	0.09	0.42	0.10	0.01	0.28	0.13
MgO	2.75	3.05	3.09	2.88	3.09	3.09	2.66	3.67	2.42	2.52	4.39	3.79	2.98	3.57	3.14
CaO	0.03	0.18	0.04	0.06	0.06	0.06	0.13	0.13	0.13	0.12	0.12	0.08	0.21	0.09	0.10
Na_2O	0.07	0.03	0.14	0.02	0.06	0.13	0.02	0.03	0.01	0.02	0.04	0.02	0.04	0.03	0.05
K_2O	6.25	6.22	7.26	6.41	7.12	6.94	5.90	7.66	5.43	6.02	4.78	7.66	6.49	4.04	6.30
Total	89.68	91.07	92.98	88.61	92.05	92.46	93.12	93.46	95.09	93.04	92.53	92.71	88.26	91.19	91.87
Site C															
Si	7.06	7.29	7.30	7.26	7.38	7.41	7.17	7.61	7.75	7.80	6.87	8.01	7.81	7.17	7.42
$Al^{(IV)}$	0.94	0.71	0.70	0.74	0.62	0.59	0.83	0.39	0.00	0.00	1.13	0.00	0.19	0.83	0.55
Total	8.00	8.00	8.00	8.00	8.00	8.00	8.00	8.00	7.75	7.80	8.00	8.01	8.00	8.00	7.97
Site B															
Ti	0.00	0.00	0.00	0.00	0.00	0.00	0.00	0.00	0.00	0.00	0.15	0.00	0.00	0.10	0.02
$Al^{(VI)}$	0.27	0.50	0.48	0.55	0.59	0.63	0.68	0.83	1.18	1.25	1.27	1.35	1.45	1.74	0.91
$Fe^{(3+)}$	2.25	1.95	1.89	1.89	1.78	1.73	1.84	1.43	1.45	1.26	1.22	0.78	0.79	0.77	1.50
$Fe^{(2+)}$	1.29	1.24	1.23	1.25	1.24	1.24	1.34	1.12	1.44	1.40	0.85	1.10	1.25	1.07	1.22
Mn	0.01	0.01	0.02	0.01	0.01	0.01	0.01	0.02	0.00	0.01	0.06	0.01	0.00	0.04	0.02
Mg	0.70	0.75	0.74	0.73	0.75	0.74	0.65	0.86	0.56	0.59	1.09	0.88	0.74	0.89	0.76
Total	4.52	4.44	4.38	4.44	4.37	4.37	4.52	4.26	4.63	4.51	4.64	4.13	4.24	4.61	4.43
Mg/(Mg+Mn+Fe)	0.35	0.37	0.37	0.37	0.37	0.37	0.32	0.43	0.28	0.30	0.54	0.44	0.37	0.45	0.38
Fe/(Fe+Al)	0.89	0.80	0.80	0.77	0.75	0.73	0.73	0.63	0.55	0.50	0.49	0.37	0.35	0.31	0.62
Site A															
Ca	0.01	0.03	0.01	0.01	0.01	0.01	0.02	0.02	0.02	0.02	0.02	0.01	0.04	0.02	0.02
Na	0.02	0.01	0.04	0.01	0.02	0.04	0.01	0.01	0.00	0.01	0.01	0.01	0.01	0.01	0.01
K	1.35	1.31	1.50	1.39	1.48	1.43	1.23	1.54	1.07	1.21	1.01	1.53	1.38	0.86	1.31
Total Site A	1.38	1.35	1.55	1.41	1.51	1.48	1.26	1.57	1.09	1.24	1.05	1.55	1.44	0.89	1.34

stage cement in pores. In thin section the mineral is green with bluegreen/yellowgreen pleochroism and high (mica-type) birefringence. Microprobe analyses (Table 1) show high total Fe contents (13–25 wt.% FeO_{tot}) and an average composition corresponding to ferroceladonite (Li et al., 1997) in terms of Mg^{2+}/Fe^{2+} and $Fe^{3+}/^{[6]}Al$. A site occupancy averages only 1.36 Atoms/22O, indicating possible nontronitic intercalations.

Adularia is a common mineral in breccia lithologies in the higher areas (>2000 m) and in the latest stage, forming idiomorphic crystals up to 5 mm in size (Fig. 3a,b). Adularia forms independent crystals, sometimes on sediments (Fig. 3b), but also occurs as overgrowths of granitic K-feldspar in wall-rock fragments. Based on 500 microprobe point analyses, the composition of adularia is nearly stoichiometric, averaging 16.75% K_2O and containing low Na_2O concentrations (0.15%) and traces of FeO (0.03%), with Ba below detection. This nearly pure K-feldspar is significantly different from that of adularia in Alpine fissures, where high amounts of Ba (0.5–6%) and Na (0.5–2.5%) are frequently present (Weibel, 1957; Nissen, 1967; Soom, 1986).

Fluorite was only found in a single sample but clearly belongs to the breccia mineralization as it occurs between different chalcedony layers. "Botryoidal" cavities in some other samples possibly are due to dissolved former fluorite.

Pyrite and marcasite are the most abundant sulfide minerals. Pyrite occurs in grain sizes from <1 μm to about 1 mm (typically around 25 μm), the larger grains are clearly euhedral (Fig. 3h). Much pyrite is extremely fine-grained (submicrometric). Marcasite is less common but occurs as inclusions in larger pyrites in breccia matrices and most abundant as idiomorphic crystals (up to 130 μm) in late stage quartz cements. Pseudomorphs of mixed pyrite/marcasite after a tabular, apparently hexagonal mineral (up to 70 by 700 μm, most likely pyrrhotite) are quite common (Fig. 3g,h). Inclusions of a tabular, but extremely thin (<1 μm) mineral are also present in pyrite. Microprobe analyses (Table 2) show that pyrite is an important host for As (mean of 57 analyses: 2.4%) but not for Sb (mean 0.09%). Arsenic in pyrite is strongly zoned.

Mo-sulfide is contained in many samples of the Grimsel Breccia as a black submicrometric pigment susceptible to oxidation. Black pigmentation is not well correlated with the occurrence of fine-grained pyrite, but with high Mo-concentrations as measured by INAA on small chips.

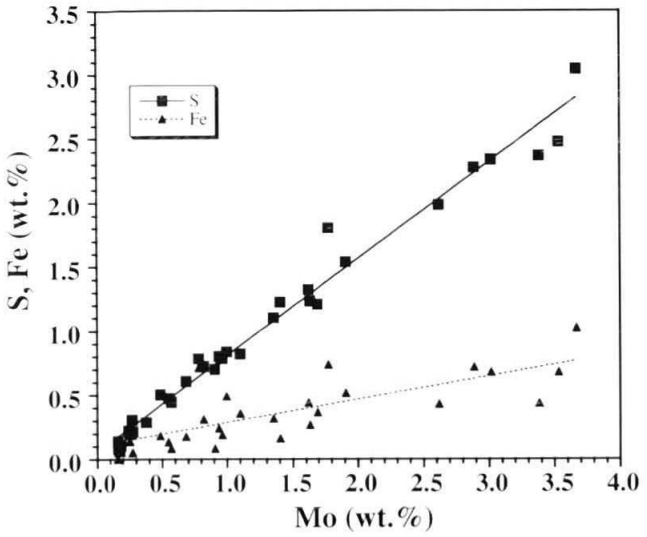

Fig. 4 Plot of Mo versus S and Fe for individual microprobe analyses of breccia matrix samples. Correlations indicate the presence of a Mo–(Fe?)-sulfide. Plotted analyses were selected from a large number of matrix analyses with the criteria Mo>0.1% and Fe<Mo.

Electron microprobe analyses of Mo-rich pigmented areas show a strong positive correlation of the concentration of Mo with S (r=0.99) and Fe (r=0.79) (Fig. 4). The correlations indicate atomic ratios corresponding to $Mo_1Fe_{0.31}S_{2.27}$, indicative of the presence of molybdenite with some associated FeS or of an Fe-bearing Mo-sulfide such as the ill-defined "femolite" of Skvortsova et al. (1964). This extremely fine-grained mineral occurs finely disseminated, but preferentially as coating on small clasts. In thin section, submicrometric Mo-sulfide is characterized by a dark-brown-olive color, clearly distinctive from pyrite-rich areas, which are purely "black-and white" in transmitted light.

Table 2 Microprobe data for pyrite.

	x	s	min	max
Pyrite from a single sample (GR1), n=30				
Fe	43.04	1.13	40.55	45.10
Co	0.01	0.02	0.00	0.07
Ni	0.01	0.02	0.00	0.07
Cu	0.04	0.05	0.00	0.20
As	1.88	1.51	0.00	5.15
Se	0.02	0.02	0.00	0.05
Sb	0.04	0.07	0.00	0.27
Tl	0.00	0.00	0.00	0.00
S	51.22	1.50	45.95	53.29
Total	96.26	1.41		
Various pyrites from breccia matrix analyses, n=27				
Fe	45.21	1.24	43.60	48.15
As	3.07	2.19	0.00	6.04
Sb	0.15	0.16	0.00	0.46
Mo	0.08	0.06	0.00	0.21
S	51.06	1.52	48.80	53.50
Total	99.58	0.96		

x — mean
s — standard deviation
min — lowest observed value
max — highest observed value

Uraninite occurs as an extremely fine-grained precipitate in the quartz-rich matrix of uranium-rich breccias. Microprobe analysis of U-rich areas resulted in a few analyses with high U concentrations (50, 63, 69%), these are very low in Th (below detection) and Ti (max. 0.02%) and as low as 0.7% in Si, strongly indicating the presence of uraninite and not of another reduced U phase such as coffinite or brannerite.

4.4. Geochemistry

Geochemical analyses were performed on three types of samples: (A) kilogram-sized bulk samples of breccias (n=20) and samples of host rocks (n=8) collected in the vicinity of the breccias to determine the overall element concentrations in breccias relative to host rocks. (B) "chip samples" (small breccia fragments) selected to represent specific (still macroscopically discernable) lithologies within the breccias, typically richer in hydrothermal phases than bulk breccias. Chip samples were analyzed to determine the major structural hosts of trace elements. These samples ranged from 0.03 to 12g in weight (mean 2.1±2.0g). C) 6 samples of recent precipitates (rich in microbial biomass) from springs in the Transitgas-tunnel. These samples were analyzed to characterize the element inventory recently deposited from the active thermal springs.

The geochemical data for bulk rocks and chip samples are presented in Appendices 2 and 3 and summarized in Tables 3 and 4, respectively. Data for recent spring deposits are shown in Appendix 2 and Table 5. Enrichment factors of mean concentrations relative to average unmineralized host rocks are shown in Table 6. Host rocks show normal crustal concentrations for all elements. The results for breccia samples demonstrate that the following elements are enriched in the Grimsel Breccia by a factor of up to 32 in bulk samples and up to 500 in chip samples: Mo, As, Sb, Au, Cs, Tl, Li, Co, Hg, U, W, Rb. Immobile lithophile elements such as Al, Sc, Nb, REE, Ta and Th are depleted in the breccia due to the presence of trace element-poor hydrothermal quartz. Ta and Th concentrations average 63 and 71% of that present in the host rock, indicating an average contribution of approximately 65% of host rock material in the breccias. Four different types of chip samples (breccia components, U-rich breccia components, chert/sediments, celadonitic cherts/sedi-

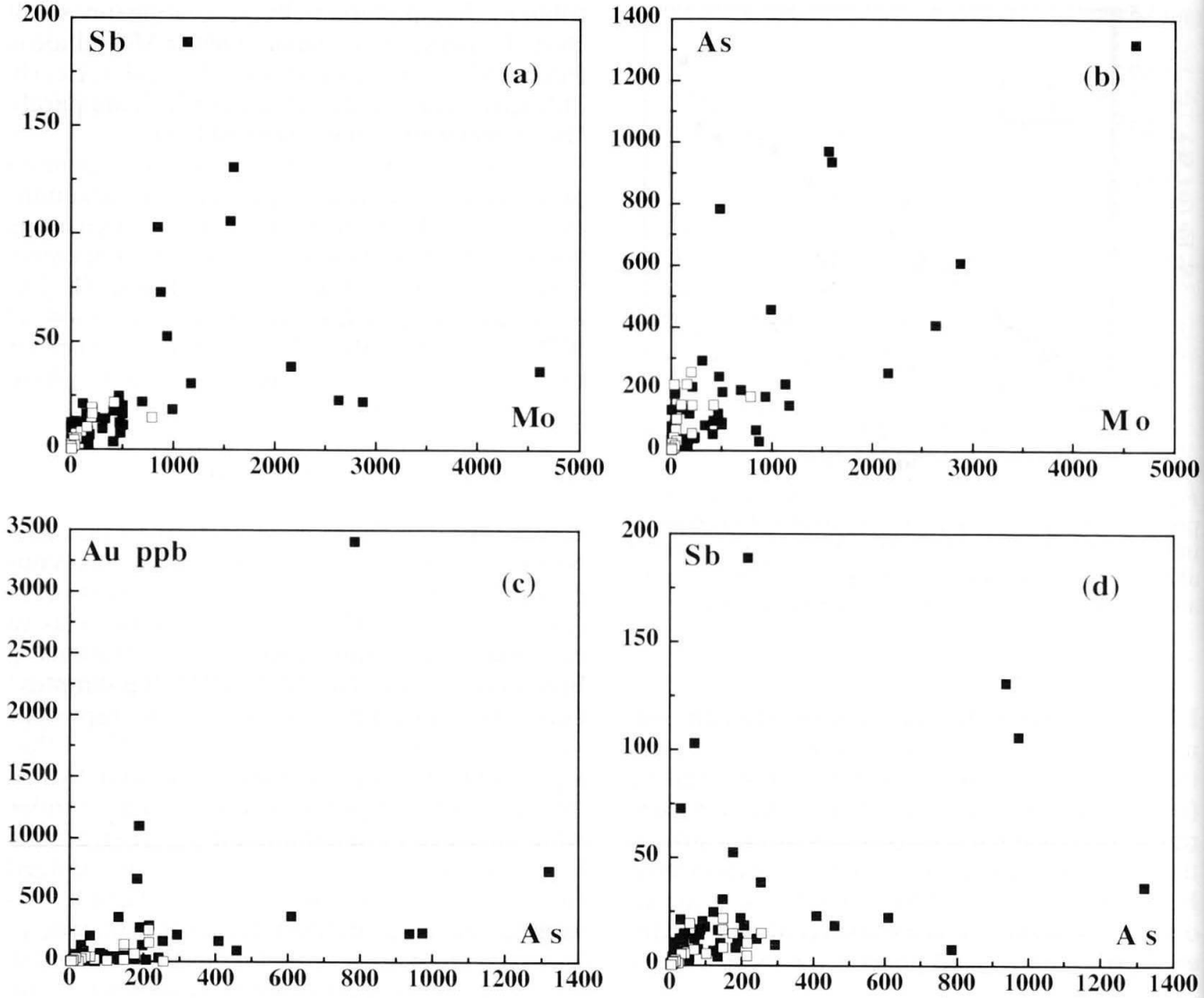

Fig. 5 Scatterplots of bulk (empty squares) and chip sample data (filled squares) for elements most strongly enriched in the Grimsel Breccia. At lower concentrations, elements are positively correlated, at higher concentrations patterns are rather erratic. Concentrations in ppm except for Au (ppb).

ments) were averaged individually (Table 4). Sediments and cherts show the highest trace element concentrations. Celadonitic cherts/sediments have lower trace element concentrations than dark (sulfidic) types. As/Sb ratios (Tables 3,4) are highly variable indicating different host phases but averages are similar for the different entities. Increased U/Th and W/Th ratios in the breccia (Tables 3, 4) indicate that U and W are enriched in the breccia relative to immobile elements even where absolute concentrations are similar to that in host rocks. Based on Ta and Th, microsamples contain an average of 45% (breccia components), 35% (sediments) and 65% (celadonitic sediments) of host rock material. Three microsamples of U-rich breccias are particularly rich in Co, As, W and also in Th. Recent spring deposits are characterized by strong enrichments of some of the same elements as the breccia (Sb, Cs, Au, Hg), while Mo, so prominent in the Grimsel Breccia, is not significantly enriched. The As/Sb ratio is much lower than in the breccias. Concentrations of immobile lithophile elements (Al, Sc, Ti, Nb, REE, Th) are surprisingly high (similar to or higher than average host rocks), indicating possible colloidal transport.

Statistical analysis of both bulk sample and chip analytical data shows significant correlations between the enriched elements, e.g. As–Au, Tl, Sb, Mo, and also between immobile elements such as Na, Sc, REE, Ta, Th, reflecting various degrees of dilution by hydrothermal minerals (correlation matrices for bulk and chip samples in Table 7). Factor analysis indicates that there are possibly two factors correlated with the enriched elements, one dominated by Mo–Tl–Sb–As and a second one with Au–Li–F–As–Fe. Scatterplots of both bulk and microsample data for the main enriched elements (Fig. 5) illustrate the highly irregular be-

haviour especially at high concentrations. The recognition of regional element concentration trends is complicated by the fact that along the outcrop there is a systematic decrease of altitude from west to east. Sb, As and Hg appear to be enriched in the higher western part, while immobile lithophile elements are negatively correlated with altitude, indicating a lower contribution of hydrothermal minerals in the eastern breccia samples. The effect of recent weathering on mineralized breccias is estimated from two pairs of microsamples representing each fresh and weathered portions of two breccia samples. The only drastic change seen is a loss of 60 and 83% of Mo during weathering, consistent with the known mobility of this element under oxidizing conditions. Two soil samples taken near the subthermal spring at Gletsch (GR 118, 119) show no anomalous element concentrations with the exception of increased Hg (0.17 ppm) in the sample taken directly at the spring, where the possibility of contamination must be considered.

4.5. Stable isotopes

4.5.1. Oxygen and hydrogen

Seven quartz samples and one adularia from the breccia are characterized by $\delta^{18}O$ values ranging from 0.89 to 9.42‰ SMOW (mean and standard deviation: 5.3±2.6‰; see Table 8), significantly lighter than the youngest phase of Alpinotype quartz (average 12.0±1.2‰) in nearby fissures. Our result for Alpinotype quartz agree with those of Mullis et al. (1994), who found a range of $\delta^{18}O$ of 10–18‰ for 5 samples of Aar massif Alpinotype quartz. Our Alpinotype quartz values correspond to a fluid $\delta^{18}O$ of +5‰ at 300 °C. A decrease of nearly 10‰ is found in the analyzed samples of breccia-stage chalcedony on Alpinotype quartz (GR44). The quartz-water and alkali feldspar-water calibrations of Matsuhisa et al. (1979) applied to adularia–quartz yields formation temperatures of 80–148 °C (mean 105±26) when samples GR44.2 and GR4B1 are omitted. The former is early breccia quartz probably formed at higher temperatures and the latter yields an unrealistically low temperature of 23 °C, perhaps due to contamination with detrital quartz. Using a formation temperature of 105±26 °C, the corresponding fluid had a $\delta^{18}O$ of approximately –15±3‰. Allowing for a precipitation of some quartz at higher temperatures (160 °C) as indicated by fluid inclusions, the possible fluid range extends up to –8‰.

Hydrogen stable isotopes were measured on three samples of clay-rich sediments/cherts and on 2 samples from Alpinotype fissures for comparison. The breccia samples are strongly depleted in deuterium relative to the Alpine fissure minerals (by 49–103‰). Assuming a formation temperature of 300 °C for the Alpinotype minerals, the following δD values can be obtained: –10 to –20‰ for water in equilibrium with chlorite (assumed fractionation: –30 to –40 ‰, Graham et al. (1987) and –30 to –40‰ for water in equilibrium with muscovite (assumed fractionation: –25±5‰, Sheppard and Gilg, 1996). For the breccia samples, fluid values of –88 to –137‰ (average –110‰) are obtained (assumed fractionation: –25±5‰, Sheppard and Gilg, 1996). Inferred oxygen and hydrogen isotopic compositions for fluids in Alpinotype fissures, the breccia, and recent waters are shown in Figure 6.

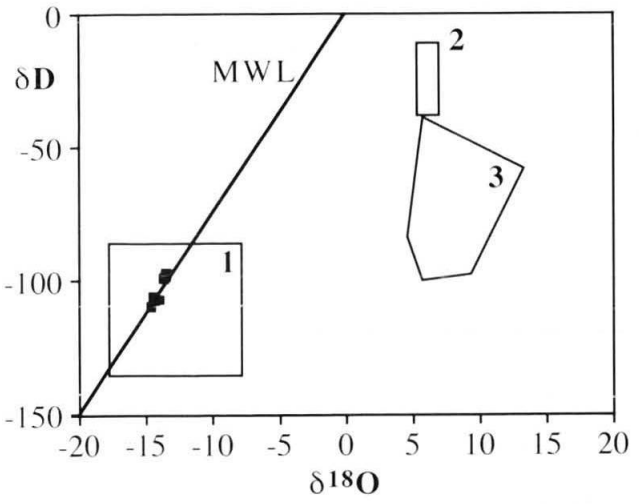

Fig. 6 Plot of $\delta^{18}O_{SMOW}$ *vs.* δD_{SMOW} for three generations of fluids in the Grimsel area. Box 1: Calculated Pliocene hydrothermal water during formation of the Grimsel Breccia (cross marks mean). Boxes 2 and 3: Fluid in alpintotype fissures based on results from this paper (2) and Mullis et al. (1994) (3). Squares show values of recent surface water and thermal springs on the Grimsel pass (isotopically lighter values are thermal waters, data from Pfeifer et al., 1992).

4.5.2. Sulfur

Sulfur stable isotopic compositions were determined on 19 samples of pyrite and sulfide-rich concentrates from the hydrothermal breccia, 15 regional reference samples and two samples of sulfate precipitated from water samples from the Gletsch subthermal spring (Table 9). Breccia sulfides (dominantly pyrite) show little variation with an average $\delta^{34}S$ of –1.7±2.6‰ (median –2.1), a few permil lighter than the regional sulfides (mean 3.9±3.2‰, median 3.6). The regional sulfides show little difference between pre-Alpine sulfides in gneisses and granite (2.1±2.3‰,

n=6) and sulfides from alpintotype fissures (5.0±3.2‰, n=9). The Gletsch subthermal spring sulfate is much heavier (16.6‰) and similar to Middle Triassic evaporites with values typically between 17 and 21‰ (Pearson et al., 1991).

4.6. U–Pb and U-series data

Four fragments of 15 to 109 mg of a uranium-rich breccia sample were selected, based on their high bulk radioactivity, for U–Pb isotopic analysis.

Table 3 Summary of bulk rock analytical data for breccias and host rocks. Elements arranged in order of decreasing enrichment in Grimsel breccia.

			Grimsel Breccia (n=20)				Host rocks[1] (n=7)				Enrichment Factor[2]
	Method		x	s	min	max	x	s	min	max	
Mo	ICP/INAA[3]	ppm	120	189	4	787	3.7	0.7	3	5	32.2
As	INAA	ppm	85	83	2	255	2.8	1.9	0.5	5.6	30.5
Sb	INAA	ppm	7.3	6.8	0.3	22	0.3	0.2	0.1	0.6	26.9
Au	INAA	ppb	49	68	1	255	<2	–	<2	4	>24.3
Cs	INAA	ppm	16	13	2	64	2.7	1.8	0.9	6.5	5.9
Tl	AA	ppm	5.5	6.6	1.1	29	1.0	0.3	0.6	1.5	5.6
Li	ICP	ppm	74	56	<1	143	14	11	5	35	5.2
Co	ICP	ppm	16	11	2	33	3.4	1.5	2	6	4.7
Hg	AA	ppb	32	55	5	260	<10	–	–	–	>3.2
U	INAA	ppm	22	52	3.4	241	8.4	3.2	3.8	13	2.6
W	INAA	ppm	3.7	1.0	1.0	5.0	2.3	0.8	1	3	1.6
Rb	INAA	ppm	283	106	140	597	185	53	120	260	1.5
Ni	ICP	ppm	5.0	5.4	0.5	20	4.6	2.0	3	9	1.1
Pb	ICP	ppm	7.1	5.8	1.0	20	7.4	4.8	1	17	1.0
V	ICP	ppm	9.7	8.3	0.5	35.0	11	6	5	20	0.9
Ca	ICP	%	0.19	0.27	0.01	1.14	0.22	0.14	0.11	0.48	0.9
Mn	ICP	ppm	217	171	47	622	269	103	48	370	0.8
Fe	ICP/INAA[3]	%	0.92	0.35	0.38	1.63	1.15	0.41	0.57	1.75	0.8
Ti	ICP	%	0.07	0.06	0.01	0.21	0.09	0.06	0.02	0.17	0.8
F	ISE	ppm	362	770	56	3600	471	577	49	1700	0.8
K	ICP	%	1.99	1.18	0.12	3.64	2.61	0.39	2.12	3.09	0.8
Zn	ICP	ppm	15	9	5	43	21	7	11	31	0.7
Cu	ICP	ppm	3.5	2.6	0.5	8	4.7	1.0	4	6	0.7
Ta	INAA	ppm	1.6	0.9	0.3	3.4	2.2	0.7	1.4	3.3	0.7
Sc	INAA	ppm	2.9	1.0	1.7	5.0	4.4	1.0	2.5	5.2	0.7
Sm	INAA	ppm	3.2	1.3	1.6	6.4	4.8	0.8	3.7	5.9	0.7
Th	INAA	ppm	15	6	6	29	24	6	15	32	0.6
Mg	ICP	%	0.11	0.11	0.01	0.46	0.22	0.10	0.09	0.39	0.5
Y	ICP	ppm	12	6	5	31	24	5	18	30	0.5
Sr	ICP	ppm	42	38	2	162	84	21	67	114	0.5
Al	ICP	%	3.23	2.12	0.22	7.58	6.67	0.67	5.49	7.64	0.5
La	INAA	ppm	17	10	6	47	36	11	22	49	0.5
Ce	INAA	ppm	30	19	3	75	64	18	39	88	0.5
Nb	ICP	ppm	8	5	0.5	19	17	5	9	25	0.5
Ba	ICP	ppm	269	219	11	826	594	82	459	682	0.5
Na	ICP/INAA[3]	%	0.82	0.66	0.11	2.64	2.81	0.55	2.30	4.01	0.3
B	ICP	ppm	<10	–	<10	14	11	0.5	<10	12	
As/Sb			12.7				11.3				
U/Th			1.47				0.35				
W/Th			0.25				0.10				

x — mean; s — standard deviation; min — lowest observed value; max — highest observed value

[1] Analyzed host rocks: 3 samples of Southern Aar Granite; 4 gneisses from the gneiss-schist-zone

[2] Mean enrichment factor: average of Grimsel Breccia/average of host rocks; calculated from unrounded values

[3] ICP and INAA data averaged for each sample

The following elements were searched for in the Grimsel breccia but were not detected (detection limit in ppm if not otherwise noted; number of analyzed samples given if not whole suite analyzed):
Se<5, Ag<2, Cd<5, Sn<20, Te<0.2(n=5), Bi<5, Pd<1ppb(n=5), Pt<5ppb(n=5)

Table 4 Summary of chip sample analytical data (INAA).

		Breccia components (n=33)				U-rich breccia (n=3)				Sediments, cherts (n=9)				Celadonite-rich sediments (n=13)			
	Unit	x	s	min	max	x	s	min	max	x	s	min	max	x	s	min	max
Na	%	0.48	0.36	0.02	1.51	0.71	0.70	0.21	1.20	0.30	0.16	0.07	0.57	0.75	0.56	0.05	1.61
Sc	ppm	3.2	2.2	0.3	10.0	2.3	1.0	1.5	3.4	3.5	0.8	1.8	4.2	2.8	1.4	0.5	5.26
Fe	%	0.92	0.58	0.29	2.70	2.45	1.10	1.50	3.65	1.24	0.37	0.56	1.78	1.04	0.72	0.32	2.70
Co	ppm	3.8	3.3	0.1	14.0	n.a.	n.a.	n.a.	n.a.	6.0	8.5	1.4	28.2	3.4	6.8	0.28	25.4
As	ppm	152	181	5	784	1867	766	1080	2610	447	489	30	1320	40	40	2	140
Rb	ppm	302	88	122	522	495	142	350	634	215	52	113	280	248	109	140	561
Mo	ppm	463	683	2	2870	n.a.	n.a.	n.a.	n.a.	1498	1309	218	4610	54	118	1	410
Sb	ppm	14	11	0	52	194	93	89	266	78	59	11	189	5	4	1	13
Cs	ppm	30	31	7	179	18	10	8	28	20	6	9	30	28	20	12	74
Ba	ppm	236	133	75	767	n.a.	n.a.	n.a.	n.a.	225	154	65	410	269	292	25	1140
La	ppm	11.4	5.2	4.1	23.0	n.a.	n.a.	n.a.	n.a.	12.3	7.3	4.7	25.0	18.0	8.1	1.91	30.5
Ce	ppm	25	10	8	50	n.a.	n.a.	n.a.	n.a.	26	14	11	53	37	17	5	64
Sm	ppm	2.4	1.2	0.1	6.3	n.a.	n.a.	n.a.	n.a.	2.4	0.7	1.5	3.6	3.6	1.8	0.1	5.81
Ta	ppm	1.0	0.7	0.1	3.5	n.a.	n.a.	n.a.	n.a.	0.7	0.4	0.2	1.2	1.5	1.0	0.07	2.96
W	ppm	1.9	1.4	0.2	6.5	13.5	4.9	10.0	17.0	1.4	1.0	0.3	2.8	2.3	3.8	0.5	14.9
Au	ppb	214	617	1	3410	194	116	91	320	237	214	19	742	35	58	1	208
Th	ppm	10	6.0	0.1	24	33	8.3	25	41	8.2	3.7	2.1	14	15	8.4	1.6	27
U	ppm	21	53	0.8	255	3864	3955	922	8360	8.6	8.1	1.5	22	13	4.9	4.8	20
As/Sb	(11.3)[1]		10.9				9.6				5.7				8.0		
U/Th	(0.35)[1]		2.0				118				1.05				0.89		
W/Th	(0.10)[1]		0.18				0.41				0.17				0.16		

x — mean; s — standard deviation; min — lowest observed value; max — highest observed value;
n.a. not quantified because of analytical problems due to high U concentration
[1] In parentheses: Host rock value from Table 3 for comparison

Table 5 Summary of analytical data for recent thermal spring deposits. Samples of microbial mats and fluffy sediment, Transitgas-tunnel (n=6). Elements are arranged in order of decreasing enrichment factors[1].

	method		x	s	min	max	Enrichment Factor[1]
Au	INAA	ppb	248	173	68	490	124
Sb	INAA	ppm	23	8	12	31	77
Cs	INAA	ppm	206	184	22	492	76
Mn	ICP	ppm	>13000	3830	4050	>20000	>48
Hg	AA	ppb	382	323	71	836	38
Pb	ICP	ppm	172	89	61	272	23
Zn	ICP	ppm	325	287	103	810	16
Ca	ICP	%	3.4	2.2	0.84	6.09	15
Cu	ICP	ppm	53	35	17	94	11
As	INAA	ppm	32	22	2	57	11
U	INAA	ppm	83	33	42	114	9.9
Fe	ICP/INAA[2]	%	6.64	2.7	2.06	10	5.8
Mg	ICP	%	1.0	0.5	0.71	1.79	4.6
Li	ICP	ppm	69	34	47	119	4.2
Tl	AA	ppm	3.7	1.4	2.6	5.7	3.7
Co	ICP	ppm	11.5	4.5	8	18	3.4
Sr	ICP	ppm	273	139	92	398	3.2
Ni	ICP	ppm	13.3	4.6	8	18	2.9
V	ICP	ppm	30	12	20	47	2.7
Ti	ICP	%	0.22	0.11	0.14	0.38	2.4
Rb	INAA	ppm	409	259	160	746	2.2
Sm	INAA	ppm	8.6	4.6	4.9	17	1.8
Sc	INAA	ppm	6.8	1.2	5.1	8.6	1.6
Mo	ICP/INAA[2]	ppm	6	3.1	2	9	1.6
Y	ICP	ppm	33	12	23	51	1.4
B	ICP	ppm	14.5	4.9	11	18	>1.3
Th	INAA	ppm	31	9	22	48	1.3
Ta	INAA	ppm	2.1	0.8	1.4	3.1	1.0
Ba	ICP	ppm	529	169	391	820	0.9
Ce	INAA	ppm	57	9	44	65	0.9
Al	ICP	%	5.2	1.6	3.5	7.21	0.8
K	ICP	%	1.8	0.3	1.53	2.07	0.7
La	INAA	ppm	26	7	17	36	0.7
Nb	ICP	ppm	10	6	7	19	0.6
F	ISE	ppm	231	90	167	294	0.5
Na	ICP/INAA[2]	%	1.13	0.6	0.54	2.03	0.4
As/Sb (11.3)[3]			1.4				
U/Th (0.35)[3]			2.65				

x — mean; s — standard deviation; min — lowest; max — highest observed value
[1] Mean enrichment factor: average of recent spring deposits/average of host rocks (Tab. 3)
[2] ICP and INAA data averaged for each sample
[3] In parentheses: Host rock value from Table 3 for comparison

Results are shown in Table 10. Clearly the samples contain significant amounts of highly radiogenic "common" lead with both uranogenic and thorogenic contributions. Isolated pyrite from the same sample fits into the trend, while a sample of grimselite, a recent uranyl mineral formed on tunnel walls on Grimsel granodiorite, (Walenta, 1972), shows rather "normal" lead. A $^{207}Pb/^{204}Pb$–$^{206}Pb/^{204}Pb$-plot of the 5 data points for the U-rich breccia sample yields a $^{207}Pb/^{206}Pb$ ratio of 0.0641 corresponding to 745 Ma, which cannot be meaningful in terms of breccia dating.

$^{208}Pb^{204}Pb$–$^{206}Pb/^{204}Pb$ also plots as a straight line with $^{208}Pb/^{206}Pb$ of 0.0295, indicating a U/Th ratio of the source material close to 10, much lower than measured in the breccia sample (~118). The covariations of both uranogenic and thorogenic Pb isotopes with uranium content are very similar, clearly indicating that this lead has been transported with U, possibly from progenitor U minerals in the southern Aar granite. The presence of "old" lead in the southern Aar granite is in accordance with results by Schaltegger and Corfu (1992), who found abundant Precam-

brian cores in zircon and allanite of the southern Aar granite.

Two grains from the same sample as used for U–Pb were subjected to alphaspectrometric measurements of U-series nuclides (Table 10). The data show an excess of ^{210}Pb and ^{230}Th over ^{238}U and ^{234}U. The two U isotopes are in equilibrium. These data are indicative of relatively recent U leaching with residual accumulation of ^{230}Th and probably ^{226}Ra as progenitor of ^{210}Pb. In light of these results is appears likely that the Pb/U ratios of these samples are also affected by alteration.

Table 6 Comparison of enrichment factors[1] for different sample types. Mean enrichment factors[1] (data from Tables 3-5) arranged in order of decreasing enrichment.

Breccia Large samples		Breccia components		Breccia U-rich samples	
Mo	32	Mo	125	As	667
As	31	Au	107	Sb	647
Sb	27	As	54	U	460
Au	24	Sb	47	Au	97
Cs	5.9	Cs	11	Cs	6.7
Tl	5.6	U	2.5	W	5.9
Li	5.2	Rb	1.6	Rb	2.7

Breccia sediment&chert		Breccia celadonitic cherts		Recent spring deposits	
Mo	405	Au	18	Au	124
Sb	260	Sb	17	Sb	77
As	160	Mo	15	Cs	76
Au	119	As	14	Mn	>48
Cs	7.4	Cs	10	Hg	38
Rb	1.2	U	1.6	Pb	23
U	1.0	Rb	1.3	Zn	16

[1] Mean enrichment factor: average of sample group/average of host rocks

4.7. ^{39}Ar–^{40}Ar dating

For ^{39}Ar–^{40}Ar-dating small (average size 1–2 mm) adularia crystals grown in open vugs in the Grimsel Breccia were carefully collected from a large sample (GR23, 450 m NNW of Sidelhorn). The collected crystals were handpicked under the microscope and a composite of the clearest and cleanest fragments was selected for analysis. Analysis steps 1 and 2 (800, 970 °C) show contamination by Ca and Cl, probably from fluid inclusions. The four steps from 1130 to 1600 °C yielded a well-defined plateau age of 3.30±0.06 Ma (Table 11, Fig. 7). Because the dated adularia is a late-stage druse mineral, this middle Pliocene age dates a late phase of breccia formation.

4.8. Fluid inclusions

Fluid inclusions were sought in several samples of fine-grained quartz cement, adularia, and coarser drusy quartz. Only the drusy quartz contained inclusions suitable for analysis. Assemblages of extremely small (few μm), flat, primary fluid inclusions were found on quartz growth-horizons, displaying bimodal fluid phase proportions at room temperature. Some inclusions contain only liquid water, whereas others contain liquid and approximately 10 vol.% vapour. None of the liquid inclusions nucleated vapour upon cooling to –190 °C,

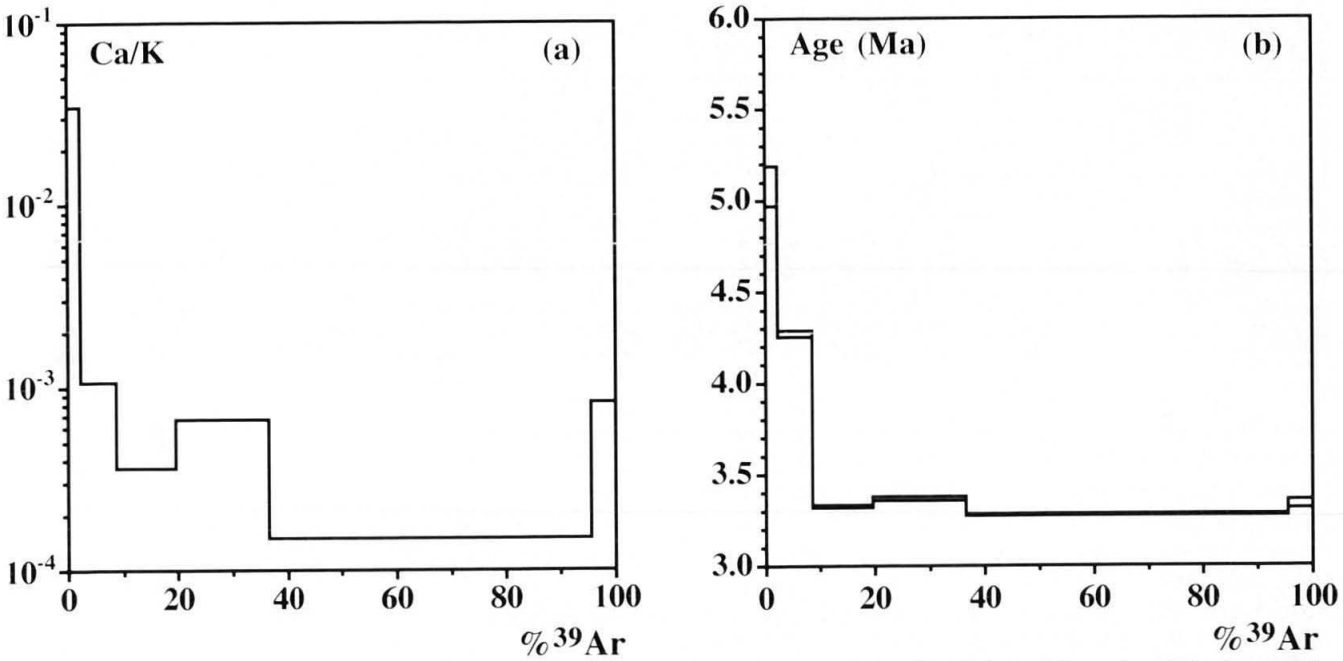

Fig. 7 Plots of Ca/K ratios and ^{39}Ar–^{40}Ar ages for different temperature steps for Grimsel Breccia adularia sample GR23.

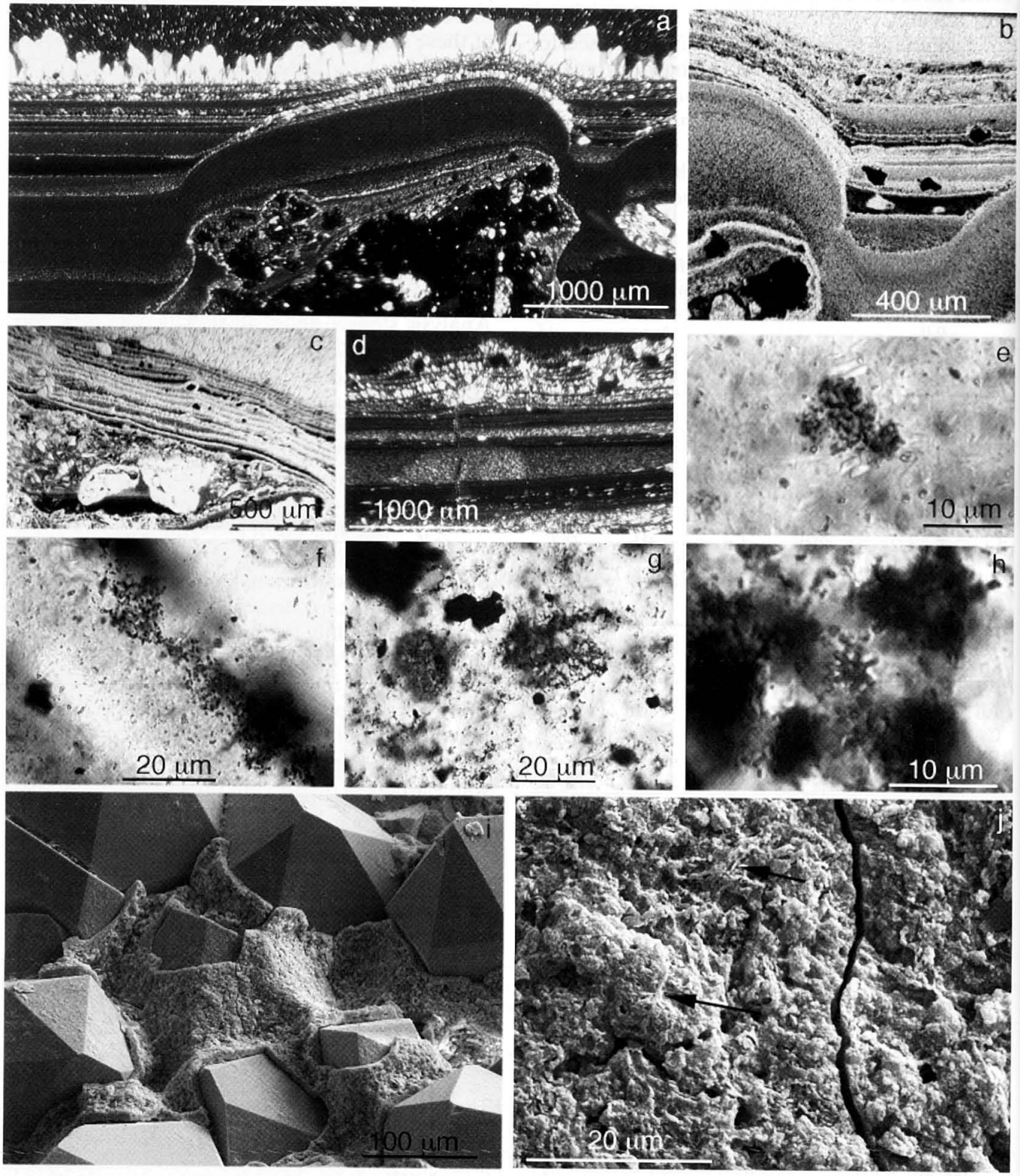

Fig. 8 Examples of Grimsel Breccia microstructures potentially related to microbial activity. (a) Thin section showing both horizontally layered geopetal infills and laminated non-horizontal deposits, crossed nicols (GR41); (b) detail of (a) showing steeply dipping and horizontally bedded fine-grained sediment, overlain by quartz layers on slope grading into sediment in flat area. Some sediment layers are nearly as thick on slopes as in flat areas, while others are absent on the slopes of the clast, indicating temporal variations in surface "stickyness"; (c) horizontally layered deposits (bottom) overgrown by undulous deposits possibly representing mineralized microbial mats (GR35); (d) fining-upwards sediment cycles covered by quartz with fine-grained horizontal layers, possibly microbial mats (GR7); (e, f) fine-grained pyrite possibly due to nucleation on microbial cells (GR4, 35); (g) same, consisting of uraninite (GR1); (h) star-shaped form (pyrite?) possibly interpretable as appendaged bacterium (GR4); (i) SEM-image of late-stage quartz overgrowth on euhedral quartz (GR82); (j) detail of (i) showing filament-like structures (arrowed).

but they are nevertheless interpreted to be metastable "stretched" liquids, due to their flatness. The temperature at which ice melts in the liquid + vapour inclusions (–0.2 °C) indicates a salinity of 0.3 wt.% eq. NaCl. Homogenization temperatures (L+V–>L) are between 130 and 150 °C, and the corresponding isochores are steep (17.5 bar/°C). Data obtained for individual inclusions are presented on Tables 12 and 13.

All the inclusions are inferred to have been trapped above 130–150 °C in the one-phase (homogeneous) liquid field (i.e. there is no fluid-inclusion evidence for boiling during breccia formation). Fluid inclusions in quartz within breccia fragments of the granitic host-rock are significantly more saline, at 6.4 – 7.1 wt.% eq. NaCl, corresponding to metamorphic fluids involved in Alpinotype fissure mineralization (Poty et al., 1974).

4.9. Search for microbial fossils and biofabrics

A search for possible microbial fossils and biofabrics was conducted by optical microscopy of thin and polished sections and by SEM investigation of the mineral surfaces in large pores and of HF-etched cross sections. This search was based on experience with other sites and published criteria (Buick, 1990; Farmer, 1999; Farmer et al., 1995; Farmer and Des Marais, 1999; Westall, 1999). No bona fide microfossils (e.g. filaments of constant diameter, well-preserved cells) were identified in the Grimsel Breccia. However, several types of observed microstructures might possibly be a result of microbial activity, even though this cannot be proven presently. Examples of structures with a biological potential are shown in Figure 8. They comprise:

– banded chert/quartz (BCQ) formations show clear evidence of particle agglutination (chert deposited on steep slopes), in contrast to flat-bedded geopetal infills associated with nearby slopes free of sediments. BCQ typically consist of finely laminated chert/quartz cement and may be interpreted as biofabrics resulting from the mineralization of biofilms (Fig. 8a–d)

– heterogeneous, "colony-like" distributed microcrystalline sulfides (mainly pyrite) and uraninite, e.g. as "balls" and thin coatings on clasts (Fig. 8e–g)

– shapes resembling appendaged bacteria (Fig. 8h)

– ill-preserved, filament-like structures up to 25 mm long and 1 mm wide in late-stage quartz (Fig. 8j)

– roundish shapes preserved in pyrite, less than 1 micron in diameter, containing a non-pyrite core, similar to "Blasenzellen" of Ramdohr (1975).

5. Discussion

5.1. Environment of formation of the Grimsel Breccia

The orientation parallel to major Alpine faults, and the association with tectonic fractures clearly indicates a dominantly tectonic origin of the Grimsel Breccia. The mapped spatial distribution of breccias and 2–3 oriented samples revealing shear sense from microscopic investigation indicate a dextral shear-sense during breccia formation. Together with slickenside orientation (lineation plunging 15–43° westwards) this indicates an uplift and eastward movement of the northern block relative to the southern one during breccia formation. The shear sense is consistent with that in other Alpine strike-slip faults (Steck and Hunziker, 1994). The inferred upward movement of the northern block apparently is inconsistent with general Alpine uplift patterns.

Present uplift rates of 0.9 mm/a might be influenced by glacial rebound (Gudmundsson, 1994). Based on various cooling ages, uplift rates varied between 0.5 and 1 mm/a in the Grimsel area during the past 15 Ma, with the highest values during the past 5 Ma. Based on the adularia age of 3.30±0.06 Ma and assuming a constant uplift rate of 0.9 mm/a, the Grimsel Breccia must have risen approximately 3 km since its formation. Thus the uppermost outcrops were approximately at 300 m below sea level at the time of formation. Stable isotopes yield clear evidence that the system was dominated by meteoric water of low salinity, with a $\delta^{18}O$ of the fluid between –9 and –15‰. The temperature of formation probably was in the range between 100 °C ($\delta^{18}O$ adularia–quartz) and approximately 160 °C (early fluid inclusions). At the time of formation (Pliocene) no magmatic activity did occur anywhere in the central Alps, so a relation to magmatism can be ruled out with certainty. Deep circulation of meteoric water must have been topography-driven as in the case with all active thermal springs in the Alps.

Three uplift histories appear possible (each assuming 0.9 mm/a uplift):

(A) Uplift and erosion were in equilibrium (stable peak altitude). The formation depth was 0.3 to 1.2 km below sea level (up to 3.9 km below surface), the geothermal gradient approx. 38 °C/km (present-day approx. 25 °C/km, Bodmer, 1982).

(B) Erosion was less than uplift (mountain growth), implying a formation depth of significantly less than 3 km. Light meteoric waters in such a situation of lower elevations imply a cooler climate. The geothermal gradient may have been >100 °C/km.

Table 7 Correlation matrices for bulk and chip samples. Significant correlations are highlighted in bold (97.5% confidence limit).

A) Bulk samples (n=20, enriched elements only)

LON[1]	**–0.96**												
Li	**0.48**	**–0.55**											
F	0.17	–0.26	0.26										
Fe	0.43	**–0.54**	**0.52**	0.37									
As	0.38	–0.37	**0.59**	0.14	–0.01								
Rb	0.14	–0.02	–0.17	–0.23	–0.29	0.16							
Mo	0.19	–0.22	0.24	–0.06	–0.15	**0.53**	–0.02						
Sb	**0.50**	**–0.50**	**0.51**	0.01	–0.04	**0.63**	0.19	**0.72**					
Cs	–0.43	**0.46**	0.11	0.00	0.13	0.01	0.28	–0.22	–0.15				
Au	0.05	–0.07	**0.55**	0.30	0.14	**0.62**	–0.33	0.19	0.24	0.06			
Hg	0.38	–0.30	–0.12	–0.04	–0.28	0.32	**0.68**	0.27	**0.56**	–0.20	–0.08		
Tl	0.19	–0.23	0.28	–0.06	–0.10	**0.58**	0.05	**0.96**	**0.68**	–0.16	0.11	0.23	
U	0.23	–0.13	–0.32	–0.08	–0.38	0.15	**0.72**	0.09	0.30	–0.18	–0.14	**0.95**	0.05
	ALT[1]	LON[1]	Li	F	Fe	As	Rb	Mo	Sb	Cs	Au	Hg	Tl

B) Chip samples (n=57)

Sc	0.06																			
Fe	**–0.31**	**0.50**																		
Co	**–0.33**	**0.33**	**0.60**																	
As	–0.16	0.07	**0.44**	0.19																
Rb	0.10	–0.17	–0.16	–0.27	–0.08															
Mo	–0.19	–0.02	0.16	0.23	**0.79**	–0.08														
Sb	**–0.30**	0.05	0.16	0.09	**0.43**	–0.18	**0.43**													
Cs	–0.26	–0.17	**0.35**	0.15	–0.06	**0.45**	–0.18	–0.07												
Ba	0.21	0.13	–0.21	–0.22	0.02	**0.42**	0.20	–0.07	**–0.29**											
La	**0.36**	0.25	0.10	–0.27	0.09	0.18	0.12	–0.16	–0.09	**0.49**										
Ce	**0.34**	0.27	0.17	–0.23	0.15	0.24	0.12	–0.17	–0.06	**0.47**	**0.97**									
Sm	**0.51**	0.22	–0.07	**–0.28**	0.01	0.12	–0.01	–0.14	–0.25	**0.45**	**0.68**	**0.70**								
Yb	**0.73**	0.09	–0.16	**–0.30**	–0.07	0.22	–0.18	–0.18	–0.18	0.25	**0.41**	**0.48**	**0.76**							
Ta	**0.84**	–0.05	**–0.39**	**–0.37**	–0.20	**0.30**	–0.17	**–0.28**	–0.20	**0.38**	**0.37**	**0.37**	**0.57**	**0.80**						
W	–0.25	0.27	**0.44**	0.16	–0.07	–0.05	–0.13	–0.06	0.11	–0.13	0.20	0.22	0.08	–0.18	**–0.28**					
Au	–0.04	–0.04	**0.34**	0.03	**0.49**	0.07	0.18	0.03	0.12	–0.03	0.07	0.12	–0.06	0.06	–0.02	–0.01				
Th	**0.67**	–0.07	**–0.35**	**–0.42**	–0.05	**0.33**	–0.12	–0.19	–0.27	**0.42**	**0.43**	**0.44**	**0.63**	**0.78**	**0.83**	–0.33	0.14			
U	–0.05	–0.20	0.08	–0.01	0.04	0.36	–0.12	–0.06	0.30	–0.18	–0.06	0.07	–0.21	0.17	–0.02	0.03	0.32	0.00		
ALT[1]	**–0.32**	–0.03	–0.12	0.11	0.06	0.00	0.14	**0.31**	–0.02	**–0.31**	**–0.62**	**–0.57**	**–0.43**	**–0.32**	**–0.38**	–0.12	–0.11	**–0.38**	0.11	
LON[1]	**0.36**	–0.01	0.09	–0.10	–0.02	–0.02	–0.12	**–0.34**	–0.01	0.26	**0.56**	**0.52**	**0.46**	**0.37**	**0.41**	0.09	0.10	**0.44**	–0.13	**–0.97**
	Na	Sc	Fe	Co	As	Rb	Mo	Sb	Cs	Ba	La	Ce	Sm	Yb	Ta	W	Au	Th	U	LON[1]

ALT and LON stand for altitude and eastward position (longitude) of samples along the strike of the Grimsel Breccia

Table 8 Oxygen and hydrogen stable isotope data.

sample	$\delta^{18}O$ ‰ rel. SMOW	
HZ-5	12.64	Alpine fissure quartz, youngest phase, Hinterer Zinggenstock, Grimsel
GR120.1	12.78	Alpine fissure quartz, youngest phase, S Totensee, Grimsel
GR44.1	10.71	Alpine fissure quartz, below breccia quartz overgrowth, E Trübtensee, Grimsel
GR44.2	0.89	Breccia quartz, very late stage
GR29.2	3.98	Breccia quartz early
GR29.1	6.25	Breccia quartz late
GR82.2	5.72	Breccia quartz, late stage sediment
GR4B.2	5.41	Breccia chalcedony early
GR4B.1	9.42	Breccia chalcedony late
GR122	5.34	Breccia chalcedony
GR23	–0.58	Breccia adularia
sample	**δD SMOW**	
B6240	–49 (1)[1]	Chlorite from protected Alpine fissure, Gerstenegg, Grimsel
B6449	–59 (1)[1]	Muscovite from Alpine fissure, Hinterer Zinggenstock, Grimsel
GR41	–137 (3)[1]	Illite-rich hydrothermal sediment, E Trübtensee
GR2	–123 (2)[1]	Illite-rich chert, E Trübtensee
GR114	–152 (2)[1]	Green celadonite-rich chert, 450 m WNW Gletsch

[1] In parenthes: number of repeat measurements

(C) Erosion was stronger than uplift (denudation). The formation depth exceeded 4 km. Meteoric waters imply a rather warm climate. The geothermal gradient would have been <30 °C/km.

It must be noted that geothermal gradients in fluid circulation systems will be strongly affected by advection and may significantly differ from regional gradients. While (A) and (B) both are possible, (C) implies a geothermal gradient unrealistically low in a geothermal system. Based on the oxygen isotopic record of Atlantic Ocean sediments (Calkin, 1995) the climate at 3.3 Ma likely was relatively stable and warmer than today, rendering possibility (B) unlikely as well. Also, magmatic heat sources in the upper crust possibly responsible for such a high geothermal gradient are missing at this time. We prefer, therefore, scenario (A). With a near-normal geothermal gradient, this scenario suggests relatively low flow rates, in accordance with the lack of host rock alteration.

We infer that formation of the Grimsel Breccia was induced by tectonic movements along a regional fault, allowing deep circulation of meteoric waters. Episodic tectonic rock fracturing in a porous, water-saturated fracture zone resulted in the formation of slurries, sedimentation involving particle sorting, and silica precipitation. It remains unclear whether rock material was carried in the fluid just by gravity-driven movement or by active transport due to strong currents. Sediment layers in geopetal infills typically show upwards-fining cycles, a pattern in accordance with an origin due to seismotectonic events. The presence of well-rounded grains and of clay-rich "lapilli-like" pellets is most likely attributable to processing in a fluidized medium (McCallum, 1985), most likely consisting of fragments and water during breccia formation.

While the dated adularia represents one of the latest stages of mineral formation at high altitude (2600 m), the finest chert varieties 400 m W of Gletsch are Mo-poor and possibly represent the youngest hydrothermal material observed in this study.

5.2. Geochemical evolution of the Grimsel Breccia

The suite of elements enriched in the Grimsel Breccia (Mo, Au, As, Sb, Cs, Tl, Hg, Li, U, W) is quite characteristic for epithermal systems (White, 1981). Recent near-surface hydrothermal systems in New Zealand (Krupp and Seward, 1987) and California (White, 1981) are often strongly enriched in Au, As, Sb, Cs, Tl, W and Li. Mo and U are rather uncommon elements in epithermal systems. A similar element suite including Mo and U is known from epithermal ores of the Schwartzwalder Mine in Colorado (Wallace and Whelan, 1986). A similar range of elements including Mo is also enriched in the Devonian Rhynie hot spring deposits in Scotland (Rice et al., 1995). Mo and U are typically soluble in relatively oxidized waters and we infer that the origin of these elements is rather from leaching under oxidizing conditions from granitic rocks from the Aar massiv, known for their molybdenite mineralizations (Steck and Hügi, 1970), while the rest of the elements were derived

Table 9 Sulfur isotope data.

Grimsel Breccia	$\delta^{34}S$ ‰ rel. CDT	
GR6	*–2.0*	Pyrite, idiomorphic, 0.1–0.3 mm
GR7	–6.0	Pyrite pure
GR7/2	–2.4	Pyrite+fine-grained sulfides
GR8	–2.9	Pyrite+fine-grained sulfides
GR8	*–4.1*	Pyrite idiomorphic 0.1-0.5 mm
GR8	*–2.1*	Sulfide fines
GR16	–4.1	Pyrite+fine-grained sulfides
GR16	*–0.6*	Pyrite coarse (to 1mm)
GR16	*4.1*	Sulfide fines
GR23/11	–0.4	Pyrite, in granite near breccia
GR26	–3.7	Pyrite pure, 0.8 mm single crystal
GR26	–4.7	Pyrite pure
GR26	*–1.4*	Pyrite 0.1–0.3 mm
GR26	*–0.7*	Sulfide fines
GR28	*2.9*	Pyrite, idiomorphic, to 0.3 mm
GR28	*0.7*	Sulfide fines
GR61	–2.9	Pyrite coarse fraction
GR61	–0.3	Pyrite fine fraction
GR115	–2.4	Pyrite+fine-grained sulfides
Mean	–1.7±2.6	
Median	–2.1	
Gletsch subthermal spring		
GR124	16.7	Sulfate precipitated as BaSO4, 50.6 ppm sulfate[1]
GR125	16.5	Sulfate precipitated as BaSO4, 49.3 ppm sulfate[1]
Regional sulfides for comparison		
A6502	12.7	Pyrite, large cube, Alpine fissure mineral, Oberaar, Grimsel
8418	3.5	Pyrite, Alpine fissure mineral, Juchlistock, Grimsel
B4849	4.6	Pyrite, Alpine fissure mineral, Gerstenegg, Grimsel
B4879	3.6	Galena, Alpine fissure mineral, Gerstenegg, Grimsel
7165	5.8	Galena, Alpine fissure mineral, Nollen, Grimsel
31080	6.1	Chalcopyrite, Alpine fissure mineral, Husegg, Grimsel
B8338	*1.3*	Galena, Alpine fissure KWO Oberaar
30126	*3.1*	Sphalerite, Alpine fissure KWO Oberaar
B9031	*4.4*	Sphalerite, Alpine fissure KWO Oberaar
A2592	4.4	Molybdenite, Nägelisgrätli, Grimsel
A8635	4.7	Molybdenite, Kessiturm, Grimsel
31301	*–0.4*	Molybdenite Uf Beesten, Handegg, Grimsel
A9213	3.6	Pyrite, accessory in biotite schist, Oberaar, Grimsel
U401s	*0.8*	Sphalerite, pre-Alpine mineralization in gneiss, Oberaar
U401p	*–0.3*	Pyrite, pre-Alpine mineralization in gneiss, Oberaar
average regional samples	3.9±3.2	
Median	3.6	

Values in italics were measured by Geochron Laboratories
[1] Determined gravimetrically as $BaSO_4$

from greater depth. Deposition of Mo and U can be explained as a result of mixing of relatively shallow, oxidizing waters with warmer, more reduced waters. The former presence of reduced waters is supported by the occurrence of abundant pyrite and of pyrrhotite pseudomorphs. Based on the fluid inclusion studies, it must be assumed that both the reducing and the oxidizing fluids were of low salinity. A relatively high mobility of U and Mo in the Grimsel granitic rocks under near-surface conditions is also indicated by the commonly observed near-surface weathering of molybdenite and the occurrence of molybdates and uranyl minerals in recent fractures and oxidized Alpine fissures in the Grimsel area (Walenta, 1972; Baertschi et al., 1991; Stalder et al., 1998).

Mineral hosts for the enriched elements are an incompletely characterized Mo-sulfide (Mo and possibly Tl, Sb), pyrite (As and probably Au) and phyllosilicates (Cs, Rb, Li). Hosts for some slightly enriched elements (W, Hg) remain unidentified.

Table 10 U–Pb isotopic and U series disequilibrium data.

Sample	U ppm	Pb tot ppm	$^{206}Pb/^{204}Pb$	± 2σ	$^{207}Pb/^{204}Pb$	± 2σ	$^{208}Pb/^{204}Pb$	± 2σ
GR1.1 bulk	5413	8.50	94.56	1.39	20.57	0.30	40.29	0.59
GR1.2 bulk	352	4.54	49.16	0.36	16.95	0.12	38.85	0.28
GR1.3 bulk	2377	10.23	80.70	0.31	19.41	0.07	39.74	0.15
GR1.4 bulk	2938	6.87	133.24	0.68	22.64	0.12	41.31	0.21
GR1.5 pyrite	n.d.	n.d.	26.30	0.12	16.08	0.07	40.30	0.18
A 8252 grimselite[1]	n.d.	n.d.	18.47	0.13	15.58	0.11	38.19	0.27

Activity ratios determined by alpha-spectroscopy

	$^{234}U/^{238}U$	$^{230}Th/^{234}U$	$^{210}Pb/^{238}U$	U (ppm)
GR1.6	1.00±0.07	1.49±0.31	1.61±0.12	1360
GR1.7	1.02±0.09	1.57±0.42	1.98±0.15	1010

[1] Recent formation in tunnel Gerstenegg-Sommerloch, Grimsel, on wall of grimsel granodiorite (Walenta, 1972)

Sulfide present mainly as pyrite and Mo-sulfide in the breccia was most likely introduced together with the deep reduced water and may have been responsible for the transport of Au, As, Sb and Hg. The average isotopic composition of breccia sulfides, with a $\delta^{34}S$ of –1.7‰, is not very diagnostic for the origin of sulfur. It is compatible with equilibrium fractionation between sulfide and excess Triassic sulfate ($\delta^{34}S$ 17–21‰) at temperatures of 220–260 °C. The origin of sulfide can thus be explained by a low degree of thermochemical reduction (by migrating hydrocarbons?) of Triassic sulfate at a depth of about 6 km, but a very deep sulfide source cannot be excluded. The absence of host rock alteration indicates that fluids were close to equilibrium with granitic minerals, which is also indicated by the occurrence of adularia. The relative abundance of marcasite may be related to partial oxidation of reduced sulfur (Murowchick and Barnes, 1986), consistent with the mixing model proposed to explain high Mo and U contents.

Radiogenic lead associated with U-rich breccia is not produced in situ but must have been carried together with the uranium, most likely from a common source, probably old (inherited Precambrian) U-rich accessory minerals in the Southern Aar granite. The presence of nonradiogenic lead associated with recent grimselite on tunnel walls indicates that recent uranium migration is decoupled from transport of radiogenic lead from the U source.

5.3. Inventory of Mo and Au

Even though clearly noneconomic, the large extent of the Grimsel Breccia and the presence of anomalous concentrations especially of Mo and Au warrant some speculation regarding the element inventory. With an estimated average thickness of 1 m, a length of 4 km and an average vertical extension of 400 m, the volume is 1.6×10^6 m^3 or about 4×10^6 t. Based on average concentrations of 120 ppm Mo and 48 ppb Au, the element content is about 480 t Mo and 190 kg Au. This demonstrates a significant transport potential of this system and there exists a possibility that higher concentrations of an economically interesting element (Au) were deposited in contact with reactive rocks such as carbonates. There are no indications, however, for the presence of carbonates along the strike of the Grimsel Breccia.

5.4. Relation to active thermal activity

Thermal springs are not uncommon in the Swiss Alps and range in temperature from 25 to 62 °C. Based on environmental isotopes, these springs are generally thought to be the result of topography-driven deep circulation of meteoric water. Reservoir temperatures based on geochemical thermometers are generally below 100 °C (Vuataz, 1982; Martinotti et al., 1999). The thermal springs in the Grimsel Transitgas tunnel, described by Pfeifer et al. (1992) and Pochon (1997), and the present project revealed that most likely these thermal waters are circulating within the Grimsel Breccia and associated fractured rock. These thermal springs are the highest-located ones in the Swiss Alps, indicating a strongly focused fluid path. It is tempting to interpret the presently ongoing thermal activity within the Grimsel Breccia as a late stage of the same processes that produced the breccia mineralization about 3.3 Ma ago. Also, the stable isotopic composition of recent thermal water and the inferred Pliocene thermal water are identical within the rather large uncertainties (at least both are clearly

Table 11 ^{39}Ar–^{40}Ar-data for adularia from the Grimsel Breccia (sample GR23).

Step	T (°C)	^{40}Artot (pl)	^{40}Ar* (pl)	^{39}Ar (pl)	^{39}Ar (%)	^{38}Ar (pl)	^{37}Ar (pl)	^{36}Ar (pl)	Ca/K	Cl/K	Age (Ma)
1	800	31.617±4	4.939	0.841±1	2.216	0.0280±2	0.01449±50	0.09029±37	3.447E-02	3.43E-04	5.08±0.11
2	970	19.210±1	11.921	2.415±2	6.365	0.0337±2	0.00129±24	0.02467±16	1.072E-03	6.86E-05	4.27±0.02
3	1130	21.526±16	16.162	4.203±4	11.079	0.0537±2	0.00076±29	0.01815±9	3.618E-04	4.79E-05	3.33±0.01
4	1290	30.802±3	24.982	6.417±6	16.915	0.0794±3	0.00215±74	0.01970±26	6.692E-04	7.67E-06	3.37±0.01
5	1520	104.969±4	84.750	22.371±20	58.966	0.2777±6	0.00167±31	0.06842±32	1.496E-04	1.75E-05	3.28±0.01
6	1600	14.100±6	6.523	1.692±2	4.459	0.0254±2	0.00070±44	0.02564±15	8.256E-04	9.17E-05	3.34±0.02

Total concentrations: K (from ^{39}Ar) 10.80%, Cl (from ^{38}Ar) 3.56 ppm, Ca (from ^{37}Ar) 110 ppm

Table 13 Microthermometric data of secondary fluid inclusions in wall-rock quartz, sample GR29. These alpine-fissure type inclusions formed *before* the primary inclusions in drusy vein-quartz shown in Table 12.

Inclusion assemblage	Inclusion number	T_n(Ice) °C	T_e °C	T_m(Ice) °C	T_h °C	T_n(V) °C
GR29B-K1	1	–36	–23	–4	186.7	
	2	–37	–22.7	–4	180.8	125
	3			–4.1	182.6	
	4			–4.1	182.5	
	5		–22.3	–4	181.6	122
	6		–22.4	–4	181.2	122
	7	–37	–22.9	–3.9	185.2	
	8	–37	–22.8	–4	186.2	43
	9			–4	186.2	
	10	–37	–22.7	–4	186.3	
	22				181.8	
	23				179.9	
	24				180.1	
	25				181.2	
	26				181.6	
	Count			10	15	
	Mean			–4	182.9	
	Max			–3.9	186.7	
	Min		–23	–4.1	179.9	
	Std.Dev				2.5	
GR29B-K2	11	–38	–23.2	–4.4	182.2	
	12	–37		–4.5	183.0	130
	13	–42		–4.5	182.7	130
	14	–38		–4.5	153.6	90
	15	–38		–4.6	185.3	130
	16	–38		–4.6	–	130
	19				182.5	
	20				180.6	
	21				181.5	122
GR29B-K3	17	–38	–23	–4	185.1	135
	18	–38		–4	188.6	
	27				185.1	
	28				188.9	

T_n(Ice): Temperature of nucleation of ice upon cooling (Liquid + Vapour –> Ice + Liquid + Vapour)
T_e: Temperature of apparent eutectic melting (Salt-Hydrates + Ice + Vapour –> Ice + Liquid + Vapour)
T_m(Ice): Temperature of final melting of ice upon heating (Ice + Liquid + Vapour –> Liquid + Vapour)
T_h: Temperature of homogenisation (Liquid + Vapour –> Liquid)
T_n(V): Temperature of nucleation of vapour (Liquid –> Liquid + Vapour) as observed after heating to T_h

meteoric). Our sulfur isotope data demonstrate that sulfate in recent thermal/subthermal waters with $\delta^{34}S$ of 16.6‰ (Gletsch locality, Table 9) and in the Transitgas tunnel ($\delta^{34}S$ 14.4 to 18.3‰, Pochon, 1997) cannot be explained by oxidation of either breccia sulfides or regional host rock sulfides but rather are indicative of an origin from

Table 12 Microthermometric data of primary fluid inclusions in drusy breccia quartz, sample GR29.

Inclusion assemblage	Inclusion number	T_n(Ice) °C	T_m(Ice) °C	T_h °C	T_n(V) °C	Notes
GR29A-1	1			130.3	–	Vapour failed to renucleate upon cooling after homogenisation
	2			130.5	–	Vapour failed to renucleate upon cooling after homogenisation
	3			134	–	Vapour failed to renucleate upon cooling after homogenisation
	4			137.8	–	Vapour failed to renucleate upon cooling after homogenisation
GR29B-1	29	–35	not visible	129.7	60	LV inclusion in otherwise all-liquid assemblage; Vapour failed to renucleate upon heating above T_n(Ice)
GR29C-1	2	–36	< +3.5			Metastable reappearance of vapour upon heating
	3	–36	–0.2			T_m(Ice) cycled convincingly
	4	–36	–0.2			
GR29D-1	1	–35				Vapour failed to renucleate upon heating above T_n(Ice)
	3	–33	< +5.5			Metastable reappearance of vapour upon heating
	5	–37	–0.2	151		T_m(Ice) cycled convincingly
	6	–35				Vapour failed to renucleate upon heating above T_n(Ice)
	7	–35	–0.3			
	8	–35	–0.3			
	9	–35	–0.3			
	10	–35	–0.3			
	11	–35	–0.3			
	12	–37	–0.3	152		T_m(Ice) cycled convincingly
	13	–37	–0.3			T_m(Ice) cycled convincingly

T_n(Ice): Temperature of nucleation of ice upon cooling (Liquid + Vapour –> Ice + Liquid + Vapour)
T_m(Ice): Temperature of final melting of ice upon heating (Ice + Liquid + Vapour –> Liquid + Vapour)
T_h: Temperature of homogenisation (Liquid + Vapour –> Liquid)
T_n(V): Temperature of nucleation of vapour (Liquid –> Liquid + Vapour) as observed after heating to T_h

Triassic evaporites. The $\delta^{18}O$ values of dissolved sulfates are very different (average –1.55‰, Pochon, 1997) from those of this suggested source (Triassic sulfate $\delta^{18}O$ range 10–18‰, Pearson et al., 1991), but could be explained by equilibration with isotopically light meteoric water ($\delta^{18}O$ –14.6‰) at about 150 °C.

The geochemical analyses of material deposited from the thermal springs in the Transitgas tunnel (Table 5) clearly indicate recent transport of many rare elements including Au, Cs, Sb, Hg, As prominent in the breccia. In contrast to the breccia, Mo is absent. An origin of the elements in the active thermal waters from remobilization of older breccia mineralization appears unlikely based on the reducing nature of the waters (strong H_2S smell after acidification). Present active transport from deep sources appears more likely. Active thermal springs are low in Ca, high in Si and fluoride and have a high pH, are reducing and contain sulfide (as is evident from the smell of acidified samples). Similar characteristics can be inferred for the fluids involved in mineralization of the Grimsel Breccia.

Based on the fact that all active thermal spring activity in the Alps is related to topography-driven flow, the active presence of topography-driven thermal waters in the Grimsel Breccia today, and the absence of any indication of Pliocene magmatic activity in the vicinity of the Grimsel area, we conclude that the motor of the hydrothermal system that mineralized the Grimsel Breccia was topography-driven flow of meteoric waters, with a small fraction of metamorphic waters possibly being mixed in.

5.5. Hydrothermal systems in the Grimsel area as a microbial habitat

This results presented here do not yield clear evidence of a microbial colonization of the Grimsel hydrothermal breccia at the time of its formation. Textures that may be related to biofilm-influenced sediment accretion appear as the best candidates. Conditions for microbial activity were favourable in terms of availability of chemical energy (mixing of fluids with different redox states, possible H_2-production resulting from pyrite precipitation). Temperatures may have been at or above tolerable limits (113 °C), as formation temperatures most likely ranges from around 100 to 160 °C. During Alpine metamorphism, all currently exposed rocks were thermally sterilized. Any microbial population must have been intro-

duced by water circulation, which was clearly possible because the waters present at a depth of several km were clearly meteoric. Further search for microbial activity would have to concentrate on the lowest-temperature precipitates.

6. Conclusions

We conclude that the Grimsel Breccia is the result of hydrothermal overprinting of a tectonic fault breccia. Meteoric water dominated the hydrothermal system of Pliocene age and deep, topography-driven circulation indicates the presence of a significant palaeorelief. Similar hydrothermal systems are known in rapidly uplifting mountain belts (Chamberlain et al., 1995, 2002), but are not commonly associated with transport of elements typical for epithermal systems. The breccia probably formed at a depth of 3–4 km at 100–160 °C. No clear textural or isotopic evidence was found for microbial colonization of the system. The Grimsel Breccia today still serves as a conduit for deep water circulation, indicating that the breccia provides a strongly focused and deep-ranging fluid conduit. Some of the same elements enriched in the Pliocene breccia (Au, Sb, As) are still being transported in the active thermal waters. The main phase of tectonic activity predates the crystallization of adularia in open vugs at 3.30±0.06 Ma and it is considered that the system is no danger to local hydroelectric power facilities.

Acknowledgements

This project would not have been possible without the support of numerous persons and institutions. J. Abrecht, P. Eckardt, T. Labhhart, H.-R. Pfeifer, F. Schlunegger, H.A. Stalder and A. Steck helped with various important informations and samples related to their earlier work. J.C. Hunziker and Z.D. Sharp kindly supported the use of the stable isotope laboratory at Lausanne University. Ph. Häuselmann provided analytical assistance and Chr. Böhm performed a part of the fieldwork. We thank the Transitgas AG for access to their tunnel. Reviews by H.A. Stalder, C. Rice and C. Marignac helped to improve the manuscript. This project was supported by grant 21-43191-95 of the Swiss National Science Foundation.

References

Armbruster, T., Kohler, T., Meisel, T., Nägler, T. F., Götzinger, M.A. and Stalder, H.A. (1996): The zeolite, fluorite, quartz assemblage of the fissures at Gibelsbach (Valais, Switzerland): crystal chemistry, REE patterns, and genetic speculations. *Schweiz. Mineral. Petrogr. Mitt.* **76**, 131–146.

Baertschi, P., Alexander, W.R. and Dollinger, H. (1991): Grimsel Test Site – Uranium migration in crystalline rock: Capillary solution transport in the granite of the Grimsel Test Site. *Nagra Technical Report* NTB 90-15, Nagra, Baden.

Bajo, S. and Eikenberg, J. (1999): Electrodeposition of actinides for alpha-spectrometry. *J. Radioanal. Nucl. Chem.* **242**, 745–751.

Belluso, E., Ruffini, R., Schaller, M. and Villa, I.M. (2000): Electron-microscope and Ar isotope characterization of chemically heterogeneous amphiboles from the Palala Shear zone, Limpopo Belt, South Africa. *Eur. J. Mineral.* **12**, 45–62.

Bodmer, P. (1982): Geothermal map of Switzerland. *Schweiz. geophys. Komm.*; Kümmerly und Frey, Bern.

Buick, R. (1990): Microfossil recognition in Archean rocks: An appraisal of spheroids and filaments from a 3500 M.y. old chert-barite unit at North Pole, Western Australia. *Palaios* **5**, 441–459.

Calkin, P.E. (1995): Global glacial chronologies and causes of glaciations. In: Menzies, J. (ed.): Modern glacial environments. Processes, Dynamics and sediments. Butterworth-Heinemann, Oxford, 9–75.

Chamberlain, C. P., Zeitler, P. K., Barnett, D. E., Winslow, D., Poulson, S. R., Leahy, T. and Hammer, J. E. (1995): Active hydrothermal systems during the recent uplift of Nanga Parbat, Pakistan Himalaya. *J. Geophys. Res.* **100**, 439–453.

Chamberlain, C.P., Koons, P.O., Meltzer, A.S., Park, S.K., Craw, D., Zeitler, P. and Poage, M.A. (2002): Overview of hydrothermal activity associated with active orogenesis and metamorphism: Nanga Parbat, Pakistan Himalaya. *Am. J. Sci.* **302**, 726–748

Degueldre, C., Longworth, G., Moulin, V., Vilks, P., Ross, C., Bidoglio, G., Cremers, A., Kim, J., Pieri, J., Ramsay, J., Salbu, B. and Vuorinen, U. (1989): Grimsel colloid exercise: an international intercomparison exercise on the sampling and characterisation of ground water colloids. *Nagra Technical Report* **NTB 90-01**, Nagra, Baden, Switzerland.

Dollinger, H. (1989): Petrographische und geochemische Untersuchungen des Altkristallins zwischen Nägelisgrätli und Oberaarjoch (Grimsel, Kt. Bern). Unpublished Diploma thesis, Bern University.

Eckardt, P., Funk, H. and Labhart, T. (1983): Postglaziale Krustenbewegungen an der Rhein-Rhone-Linie. *Vermessung, Photogrammetrie und Kulturtechnik.* **83/2**, 43–56.

Farmer, J. (1999): Taphonomic modes in microbial fossilization. In: Size limits of very small microorganisms. Space Studies Board, Natural Research Council, Washington, D.C., 94–102.

Farmer, J.D. and Des Marais, D. J. (1999): Exploring for a record of ancient Martian life. *J. Geophys. Res.* **104/E11**, 26977–26995.

Farmer, J.D., Cady, S. and Des Marais, D. J. (1995): Fossilization processes in thermal springs. *Geol. Soc. Am., Abstr.* with Progr. **27**, p. 305.

Frey, M. and Ferreiro Mählmann, R.F. (1999): Alpine metamorphism of the Central Alps. *Schweiz. Mineral. Petrogr. Mitt.* **79**, 135–154.

Graham, C.M., Viglino, J.A. and Harmon, R.S. (1987): Experimental study of hydrogen-isotope exchange between aluminous chlorite and water and of hydrogen diffusion in chlorite. *Am. Mineral.* **72**, 566–579.

Gudmundsson, H. (1994): An order-of-magnitude estimate of the current uplift-rate in Switzerland caused by the Würm Alpine deglaciation. *Eclogae geol. Helv.* **87**, 545–557.

Herdianita, N.R., Browne, P.R.L., Rodgers, K.A. and Campbell, K.A. (2000): Mineralogical and textural changes accompanying ageing of silica sinter. *Mineralium Deposita* **35**, 48–62.

Hofmann, B. (1989): Genese, Alteration und rezentes Fliess-System der Uranlagerstätte Krunkelbach

(Menzenschwand, Südschwarzwald). *Nagra Technical Report* **NTB 88-30**, Nagra, Baden.

Hofmann, B.A. and Farmer, J.D. (1997): Microbial fossils from terrestrial subsurface hydrothermal environments: Examples and implications for Mars. In: Clifford, S.M., Treiman, A.H., Newsom, H.E. and Farmer, J.D. (eds): Conference on Early Mars: Geologic and Hydrologic Evolution, Physical and chemical environments, and the implications for Life. LPI Contr. 916 ed. Lunar and Planetary Science Institute, Houston, 40–41.

Hofmann, B.A. and Farmer, J.D. (2000): Filamentous fabrics in low-temperature mineral assemblages: Are they fossil biomarkers? Implications for the search for a subsurface fossil record on the early Earth and Mars. *Planetary and Space Science* **48**, 1077–1086.

Hofmann, B.A. and Frei, R. (1996): Age constraints of reduction spot formation from Permian red bed sediments, northern Switzerland, inferred from U–Th–Pb systematics. *Schweiz. Mineral. Petrogr. Mitt.* **76**, 235–244.

Horwitz, E.P., Diez, M.L., Chiariza, R., Diamond, H., Essling, A.M. and Grazyk, D. (1992): Separation and preconcentration of uranium from acid media by extraction chromatography. *Analyt. chim. Acta* **266**, 25–37.

Jobson, D.H., Boulter, C.A. and Foster, R.P. (1994): Structural controls and genesis of epithermal gold-bearing breccias at the Lebong Tandai mine, Western Sumatra, Indonesia. *J. Geochem. Explor.* **50**, 409–428.

Kahle, H.-G., Geiger, A., Bürki, B., Gubler, E., Marti, U., Rothacher, M., Gurtner, W., Beutler, G., Bauersima, I. and Pfiffner, O.A. (1997): Recent crustal movements, geoid and density distribution: Contribution from integrated satellite and terrestrial measurements. In: Pfiffner, O.A., Lehner, P., Heitzmann, P., Mueller, S. and Steck, A. (eds): Deep structure of the Swiss Alps. Results of NRP 20. Birkhäuser, Basel, 251–259.

Keusen, H.R., Ganguin, J., Schuler, P. and Buletti, M. (1989): Grimsel Test Site – Geology. *Nagra Technical Report* **NTB 87-14E**, Nagra, Baden.

Kralik, M., Clauer, N., Holnsteiner, R., Huemer, H. and Kappel, F. (1992): Recurrent fault activity in the Grimsel Test Site (GTS, Switzerland): revealed by Rb–Sr, K–Ar and tritium isotope techniques. *J. Geol. Soc. London* **149**, 293–301.

Krupp, R.E. and Seward, T.M. (1987): The Rotokawa hydrothermal system, New Zealand: An active epithermal gold-depositing environment. *Econ. Geol.* **82**, 1109–1129.

Li, G., Peacor, D.R., Coombs, D. and Kawachi, Y. (1997): Solid solution in the celadonite family: The new minerals ferroceladonite and ferroaluminoceladonite. *Am. Mineral.* **82**, 503–511.

Martinotti, G., Marini, L., Hunziker, J.C., Perello, P. and Pastorelli, S. (1999): Geochemical and geothermal study of springs in the Ossola-Simplon region. *Eclogae geol. Helv.* **92**, 295–305.

Matsuhisa, Y., Goldsmith, J. R. and Clayton, R.R. (1979): Oxygen isotopic fractionation in the system quartz–albite–anorthite–water. *Geochim. Cosmochim. Acta* **43**, 1131–1140.

McCallum, M.E. (1985): Experimental evidence for fluidization processes in breccia pipe formation. *Econ. Geol.* **80**, 1523–1543.

Michalski, I. and Soom, M. (1990): The Alpine thermotectonic evolution of the Aar and Gotthard massifs, Central Switzerland: Fission Track ages on zircon and apatite and K–Ar mica ages. *Schweiz. Mineral. Petrogr. Mitt.* **70**, 373–387.

Mullis, J., Dubessy, J., Poty, B. and O'Neil, J. (1994): Fluid regimes during late stages of a continental collison: Physical, chemical and stable isotope measurements of fluid inclusions in fissure quartz from a geotraverse through the Central Alps, Switzerland. *Geochim. Cosmochim. Acta* **58**, 2239–2267.

Murowchick, J.B. and Barnes, H.L. (1986): Marcasite precipitation from hydrothermal solutions. *Geochim. Cosmochim. Acta* **50**, 2615–2630.

Niggli, C.R. (1965): Petrographie und Petrogenesis der Migmatite und Gneise im südlichen Aarmassiv zwischen Obergesteln und Furkapass. Unpubl. Doctoral Thesis, Bern, 115 pp.

Nissen, H.U. (1967): Adular aus den Schweizeralpen: Domänengefüge, Natriumgehalt, Natriumentmischung und Gitterkonstanten. *Schweiz. Mineral. Petrogr. Mitt.* **47**, 1140–1145.

Pavoni, N., Maurer, H.R., Roth, P. and Deichmann, N. (1997): Seismicity and seismotectonics of the Swiss Alps. In: Pfiffner, O.A., Lehner, P., Heitzmann, P., Mueller, S. and Steck, A. (eds): Deep structure of the Swiss Alps. Results of NRP 20. Birkhäuser, Basel, 241–250.

Pearson, F.J., Balderer, W., Loosli, H.H., Lehmann, B.E., Matter, A., Peters, T., Schmassmann, H. and Gautschi, A. (1991): Applied isotope hydrogeology. A case study in northern Switzerland. *Studies in Environmental Science* **43**. Elsevier, Amsterdam, 439 pp.

Pettke, T. and Diamond, L. (1997): Oligocene gold quartz veins at Brusson, NW Alps: Sr isotopes trace the source of ore-bearing fluids to over 10-km depth. *Econ. Geol.* **92**, 389–406.

Pettke, T., Diamond, L.W. and Kramers, J.D. (2000): Mesothermal gold lodes in the north-western Alps: A review of genetic constraints from radiogenic isotopes. *Eur. J. Mineral.* **12**, 213–230.

Pettke, T., Diamond, L.W. and Villa, I.M. (1999): Mesothermal gold veins and metamorphic devolatilization in the northwestern Alps: the temporal link. *Geology* **27**, 641–644.

Pfeifer, H.-R., Sanchez, A. and Degueldre, C. (1992): Thermal springs in granitic rocks from the Grimsel Pass (Swiss Alps): The late stage of a hydrothermal system related to Alpine Orogeny. In: Kharaka, Y.K. and Maest, A.S. (eds): 7th international Symposium on Water-Rock Interaction. Balkema, Rotterdam, Park City, Utah, USA, 1327–1331.

Pochon, A. (1997): Etude pétrographique, géochimique et structurale dans la région du col du Grimsel (BE, VS). Données hydrochimiques et isotopiques sur les venues d'eau thermale de la galerie de Transit Gas AG (pipe-line Hollande-Italie). Unpubl. Diploma thesis, University of Neuchâtel, 183 pp.

Poty, B.P., Stalder, H. A. and Weisbrod, A.M. (1974): Fluid inclusion studies in quartz from fissures of western and central Alps. *Schweiz. Mineral. Petrogr. Mitt.* **54**, 717–752.

Ramdohr, P. (1975): Die Erzmineralien und ihre Verwachsungen. 4th ed. Akademie-Verlag, Berlin, 1277 pp.

Rice, C.M., Ashcroft, W.A., Batten, D.J., Boyce, A.J., Caulfield, J.B.D., Fallick, A.E., Hole, M.J., Jones, E., Pearson, M.J., Rogers, G., Saxton, J.M., Stuart, F.M., Trewin, N.H. and Turner, G. (1995): A Devonian auriferous hot spring system, Rhynie, Scotland. *J. Geol. Soc. London* 152, 229–250.

Schaltegger, U. and Corfu, F. (1992): The age and source of late Hercynian magmatism in the central Alps: evidence from precise U–Pb ages and initial Hf isotopes. *Contrib. Mineral. Petrol.* **111**, 329–344.

Sharp, Z.D. (1990): A laser-based microanalytical meth-

od for the in-situ determination of oxygen isotope ratios in silicates and oxides. *Geochim. Cosmochim. Acta* **54**, 1353–1357.

Sharp, Z.D. (1992): In situ laser microprobe techniques for stable isotope analyses. *Chem. Geol.* **101**, 3–19.

Sheppard, S.M. and Gilg, H.A. (1996): Stable isotope geochemistry of clay minerals. *Clay Min.* **31**, 1–24.

Sibson, R.H. (1987): Earthquake rupturing as a mineralizing agent in hydrothermal systems. *Geology* **15**, 701–704.

Skvortsova, K.V., Sidorenko, G.A., Dara, A.D., Silant'yeva, N.I. and Medoyeva, M.M. (1964): Femolite – a new molybdenum sulphide. *Zapiski Vserossijskogo Mineralogicheskogo Obshchestva*, p. 93/4, 436–443.

Soom, M. (1986): Geologie und Petrographie von Ausserberg (VS). Kluftmineralisationen am Südrand des Aarmassivs. Unpubl. Diploma thesis, Bern, 129 pp.

Stalder, H.A. (1964): Petrographische und mineralogische Untersuchungen in Grimselgebiet. *Schweiz. Mineral. Petrogr. Mitt.* **44**, 187–398.

Stalder, H.A., Wagner, A., Graeser, S. and Stuker, P. (1998): Mineralienlexikon der Schweiz. Wepf, Basel, 579 pp.

Steck, A. (1968): Die alpidischen Strukturen in den Zentralen Aaregraniten des westlichen Aarmassivs. *Eclogae geol. Helv.* **61/1**, 19–48.

Steck, A. and Hügi, T. (1970): Das Auftreten des Molybdänglanzes im westlichen Aarmassiv und Molybdängehalte von Gesteinen der gleichen Region. *Schweiz. Mineral. Petrogr. Mitt.* **50**, 257–276.

Steck, A. and Hunziker, J. (1994): The Tertiary structural and thermal evolution of the Central Alps—compressional and extensional structures in an orogenic belt. *Tectonophysics* **238**, 229–254.

Valenza, K., Moritz, R., Mouttaqi, A., Fontignie, D. and Sharp, Z. (2000): Vein and Karst barite deposits in the western Jebilet of Morocco: Fluid inclusion and isotope (S, O, Sr) evidence for regional fluid mixing related to central Atlantic rifting. *Econ. Geol.* **95**, 587–606.

Vuataz, F. (1982): Hydrologie et géochimie des eaux minérales et thermales de Suisse et des régions alpines limitrophes. *Matér. Géol. Suisse. Série hydrol.* **29**. Kümmerly und Frey, Bern, 174 pp.

Walenta, K. (1972): Grimselit, ein neues Mineral aus dem Grimselgebiet BE. *Schweiz. Mineral. Petrogr. Mitt.* **52**, 93–108.

Wallace, A.R. and Whelan, J. F. (1986): The Schwartzwalder uranium deposit, III: Alteration, vein mineralization, light stable isotopes, and genesis of the deposit. *Econ. Geol.* **81**, 872–888.

Weibel, M. (1957): Zum Chemismus der alpinen Adulare (II). *Schweiz. Mineral. Petrogr. Mitt.* **37**, 545–553.

Westall, F. (1999): The nature of fossil bacteria: A guide to the search for extraterrestrial life. *J. Geophys. Res.* **104/E7**, 16437–16451.

White, D.E. (1981): Active geothermal systems and hydrothermal ore deposits. *Econ. Geol.* **75**th Ann. Vol., 392–423.

Received 6 March 2003
Accepted in revised form 1 November 2004
Editorial handling: R. Gieré

Appendix

Appendix Table 1 Samples and localities.

Sample Nr	Description	Locality	Swiss coordinates	Altitude
GR1	U-rich breccia	Trübtensee-Sidelhorn area	~667000/156400	2600
GR2	Breccia	Near Trübtensee, Oberaar	666600/156350	2450
GR3	Breccia	Near Trübtensee, Oberaar	666600/156350	2450
GR4	Breccia	Near Trübtensee, Oberaar	666600/156350	2450
GR6	Breccia	Grat 450 m NNW Sidelhorn	667125/156475	2630
GR7	Breccia	Grat 450 m NNW Sidelhorn	667125/156475	2630
GR8	Breccia	Grat 450 m NNW Sidelhorn	667125/156475	2630
GR10	Breccia	Grat 450 m NNW Sidelhorn	667125/156475	2630
GR14	Breccia	Grat 450 m NNW Sidelhorn	667125/156475	2630
GR16	Breccia, grey, dense	Near Trübtensee, Oberaar	666600/156350	2450
GR17	Cataclasite	Near Trübtensee, Oberaar	666600/156350	2450
GR18	Breccia, coarse	Near Trübtensee, Oberaar	666600/156350	2450
GR19	Biomass from thermal spring	Transitgas tunnel, spring 24	669680/156340	1920
GR20	Biomass from thermal spring	Transitgas tunnel, spring 11	669680/156360	1920
GR21	Sediment from tunnel creek near thermal spring	Transitgas tunnel, near springs 11, 24	669680/156360	1920
GR22	Breccia, block of 12.5 kg	Grat 450 m NNW Sidelhorn	667125/156475	2520
GR23	Breccia with adularia	Grat 450 m NNW Sidelhorn	667125/156475	2630
GR26	Chert	Grat 450 m NNW Sidelhorn	667125/156475	2630
GR27	Chert	800 m NW Sidelhorn	667630/156450	2520
GR28	Breccia	500 m SW Totensee	668375/156650	2220
GR29	Breccia with quartz crystals	Grat 450 m NNW Sidelhorn	667125/156475	2630
GR34	Breccia with sediment	Grat 450 m NNW Sidelhorn	667125/156475	2630
GR35	Breccia, host rock, geopetal features	Grat 450 m NNW Sidelhorn	667125/156475	2630
GR36	Brekzie with slickenside	300 m ENE Trübtensee	666460/156300	2460
GR39	Breccia, porous	650 m ENE Trübtensee	666750/156350	2520
GR41	Internal sediment from breccia	500 m ENE Trübtensee	666560/156340	2480
GR42	Breccia	500 m ENE Trübtensee	666560/156340	2480
GR44	Alpine fissure quartz, overgrown by Breccia chalcedony	500 m ENE Trübtensee	666560/156340	2480
GR46	Southern Aar granite, sheared	Sidellimmi	667875/156700	2380
GR48	Southern Aar granite, undeformed	Sidellimmi	667875/156700	2380
GR52	Breccia, dark	500 m SW Totensee	668375/156650	2220
GR53	Breccia, dark	500 m SW Totensee	668375/156650	2220
GR60	Breccia, component from breccia	680 m NE Sidelhorn	667610/156420	2470
GR61	Breccia, fine-grained	680 m NE Sidelhorn	667610/156420	2470
GR72	Southern Aar granite, undeformed	400 m E Trübtensee/500 m W Sidelhorn	666520/156100	2430
GR82	Breccia (fracture infill)	450 m N Sidelhorn	667040/156450	2600
GR84	Breccia (fracture infill, red-green, radioactive)	360 m NW Sidelhorn	666840/156370	2560
GR87	Quartzitic gneiss	480 m NW Sidelhorn (E P. 2469)	666666/156395	2470
GR88	Gneiss (breccia host rock)	520 m NNW Sidelhorn	666840/156500	2525
GR89	Gneiss (breccia host rock)	520 m NNW Sidelhorn	666840/156475	2530
GR90	Gneiss, cataclastic (breccia host rock)	450 m NNW Sidelhorn	666930/156500	2560
GR98	Biomass from thermal spring	Transitgasstollen 9145m, spring 24	669680/156340	1920
GR100	Breccia	1150 m NE Sidelhorn	668115/156590	2330
GR102	Breccia	Gletsch, close to subthermal spring (float)	670600/157280	1830
GR105	Biomass from thermal spring	Transitgasstollen 9124m, spring 11	669680/156360	1920
GR107	Biomass from thermal spring	Transitgasstollen 9145m, spring 24	669680/156340	1920
GR114	Breccia with green chalcedony	450 m WNW Gletsch	670300/157220	1900
GR115	Breccia	Meienbach S Plänggerli	669700/157070	2090
GR118	Soil sample, adjacent to subthermal spring	Gletsch subthermal spring	670720/157230	1760
GR119	Soil sample	Gletsch, above road	670700/157200	1770
GR120	Alpine fissure quartz	S of Totensee	~669900/156900	2000
GR122	Chalcedony	E of Trübtensee	666500/156200	2450
GR124	BaSO4 precipitated from spring water	Gletsch subthermal spring (15.7.1996)	670720/157230	1760
GR125	BaSO4 precipitated from spring water	Gletsch subthermal spring (15.7.1996)	670720/157230	1760
GR127	Breccia, greenish matrix	350 m WNW Gletsch	670450/157250	1880
GR128	Breccia, greenish matrix	450 m WNW Gletsch	670325/157250	1900
GR129	Breccia, greenish matrix	450 m WNW Gletsch	670325/157250	1900
GR130	Breccia, greenish matrix	450 m WNW Gletsch	670325/157250	1900
GR131	Breccia, greenish matrix, large boulder	450 m WNW Gletsch	670325/157250	1900
GR132	Breccia, greenish matrix	450 m WNW Gletsch	670325/157250	1900
GR135	Breccia, greenish matrix	150 m W Gletsch (float)	670650/157225	1820
GR137	Uranium-rich breccia	Sidelenhorn area	~667000/156400	2600
GR138	Uranium-rich breccia (Lhu 106a)	Sidelenhorn area	~667000/156400	2600
GR139	Silty infill in fracture in Gneiss	Gletsch, ca. 100 W of subthermal spring	670650/157150	1770

Appendix Table 2 Element concentration raw data for bulk samples.

				Grimsel Breccia samples													
		Sample Nr GR.		39		42			52	60	100	102	115	127	128	129	130	137
		Mill used(2)		ST	ST	ST	ST		ST	ST	ST	ST	ST	WC	WC	WC	WC	WC
El	Method		detection limit(1)															
Li	ICP	ppm	2	124	146	138	138		78	7	136	47	136	4	5	4	5	<1
B	ICP	ppm	10	bd	bd	bd	bd		13	13	11	14	13	bd	bd	bd	bd	bd
F	ISE	ppm	20	3596	267	233	*250*		105	161	238	312	119	108	116	82	91	56
Na	ICP	%	0.01	0.52	0.45	0.43	0.44		0.78	2.32	0.51	1.13	0.43	0.02	0.02	0.03	0.04	0.03
Na	INAA	%	0.02	0.58	0.5	0.52	0.51		0.9	2.77	0.63	1.4	0.53	1.2	1.3	0.8	1.1	0.86
Mg	ICP	%	0.01	0.12	0.08	0.08	0.08		0.05	0.1	0.1	0.3	0.09	0.07	0.07	0.06	0.06	<.01
Al	ICP	%	0.01	2.99	2.88	2.72	2.72		3.19	6.43	3.62	5.51	2.89	0.22	0.26	0.27	0.37	0.27
K	ICP	%	0.01	1.75	2.07	1.79	1.79		2.44	3.05	2.65	3.07	2.27	0.12	0.13	0.16	0.21	0.23
Ca	ICP	%	0.01	0.55	0.17	0.15	0.15		0.04	0.45	0.02	0.04	0.09	0.06	0.01	0.05	0.06	<0.01
Sc	INAA	ppm	0.2	2.3	2.1	2	2.05		1.7	4.5	3.3	4.4	1.9	2.3	3	1.8	2.5	1.8
Ti	ICP	%	0.01	0.08	0.08	0.07	0.07		0.03	0.08	0.06	0.05	0.03	0.01	<.01	0.01	0.02	<0.01
V	ICP	ppm	2	17	22	21	21		4	7	6	11	7	2	<1	3	2	4
Cr	ICP	ppm	2	276	299	302	302		316	200	176	143	287	26	2	3	2	3
Cr	INAA	ppm	20	540	480	550	515		520	340	330	280	480	36	<20	45	50	<20
Mn	ICP	ppm	5	110	69	64	64		109	445	180	476	150	590	141	164	193	47
Fetot	ICP	%	0.01	0.99	0.93	0.87	0.87		0.62	0.94	0.71	0.94	0.79	0.62	0.37	0.45	0.4	0.46
Fe	INAA	%	0.2	1.6	1.1	1.2	1.15		0.9	1.1	1.1	1.4	1.2	0.5	0.4	0.6	0.4	0.3
Co	ICP	ppm	1	5	3	3	3		3	3	2	2	2	24	12	30	24	33
Co	INAA	ppm	5	bd	bd	bd	bd		bd	bd	bd	bd	bd	21	7	28	16	30
Ni	ICP	ppm	1	7	6	6	6		7	6	6	4	5	19	1	2	1	2
Cu	ICP	ppm	1	7	6	5	5		6	6	4	4	5	8	<1	1	<1	1
Zn	ICP	ppm	2	15	11	9	9		8	18	13	29	10	8	11	7	11	5
Ga	ICP	ppm	2	bd	11	bd	bd		bd	11	bd	17	bd	bd	2	2	3	bd
As	ICP	ppm	5	125	189	184	184		155	bd	25	12	186	11	25	18	11	156
As	INAA	ppm	0.5	148	213	217	215		176	3.9	32	15	214	8.2	24	16	9.2	147
Se	INAA	ppm	5	bd	bd	bd	bd		bd	bd	bd	bd	bd	bd	bd	bd	bd	bd
Br	INAA	ppm	0.5	0.9	0.5	0.7	0.6		bd	bd	bd	bd	0.7	1.5	0.8	1.4	1.2	2.5
Rb	INAA	ppm	5	190	230	230	230		230	200	340	410	230	190	400	140	270	597
Sr	ICP	ppm	1	47	55	53	53		28	89	29	50	38	3	3	6	6	2
Y	ICP	ppm	5	7	6	6	6		13	31	15	16	15	5	13	7	10	7
Zr	ICP	ppm	5	bd	bd	bd	bd		7	bd	8	bd	bd	<1	<1	<1	<1	<1
Nb	ICP	ppm	5	9	10	9	9		12	19	13	17	11	2	2	2	4	<1
Mo	ICP	ppm	1	84	136	133	133		689	5	45	5	25	29	10	38	3	210
Mo	INAA	ppm	1	117	179	177	178		884	6	60	7	32	29	10	36	5	206
Pd°	FA-DCP	ppb	1											bd	bd	bd	bd	bd
Ag	ICP	ppm	2	bd	bd	bd	bd		bd	bd	bd	bd	bd	<0.2	<0.2	0.2	<0.2	<0.2
Ag	INAA	ppm	0.5	bd	bd	bd	bd		bd	bd	bd	bd	bd	bd	bd	bd	bd	bd
Cd	ICP	ppm	1	bd	bd	bd	bd		bd	bd	bd	bd	bd	<0.2	<0.2	<0.2	<0.2	0.6
Sb	INAA	ppm	0.1	8.2	10.3	10.5	10.4		14.9	0.3	5.3	2.6	4.4	1.8	1.1	2	1.5	16.7
Cs	INAA	ppm	0.5	15	15	14	14.5		6.4	2	15	63.6	27	13	20	11	18	5.2
Ba	ICP	ppm	5	281	286	271	271		405	513	483	826	244	14	13	16	18	11
Ba	INAA	ppm	50	230	240	210	225		320	470	450	750	230	220	530	190	310	180
La	ICP	ppm	5	12	15	15	15		16	33	22	12	15	3	9	5	8	7
La	INAA	ppm	2	14	15	15	15		17	38	25	13	16	12	13	14	16	6
Ce	INAA	ppm	5	20	13	22	17.5		<5	74	36	20	26	27	37	39	47	<40
Sm	INAA	ppm	0.1	1.6	1.8	1.9	1.85		2.3	5.9	3.6	2.4	2.8	2.5	3.8	2.7	3.2	6.4
Eu	INAA	ppm	1	bd	bd	bd	bd		bd	bd	bd	bd	bd	bd	bd	bd	bd	bd
Tb	INAA	ppm	0.5	bd	bd	bd	bd		0.7	1.3	0.6	0.7	0.5	bd	0.5	bd	bd	bd
Yb	INAA	ppm	2	bd	bd	bd	bd		3	4	3	3	2	bd	bd	bd	bd	bd
Lu	INAA	ppm	0.2	bd	bd	bd	bd		bd	bd	bd	bd	bd	bd	bd	bd	bd	bd
Hf	INAA	ppm	1	2	2	.	2		2	5	3	1	bd	6	3	5	6	<3
Ta	INAA	ppm	0.5	bd	bd	bd	bd		0.7	2.4	1.9	2.7	0.6	2.5	3.4	2.5	2.7	1.3
W	INAA	ppm	1	4	4	4	4		3	3	3	3	4	386	160	456	354	474
Pt	FA-DCP	ppb	5															
Au	FA-DCP	ppb	1															
Au	INAA	ppb	2	140	150	160	155		62	3	21	6	255	16	bd	26	10	15
Hg	AA	ppb	10	30	28	22	22		31	bd	11	17	bd	bd	bd	bd	bd	258
Tl	AA	ppm	0.1	4.8	6.5	7.3	7.3		29.3	1.1	2.5	2.8	2.1	1.3	2.2	1.8	1.9	7.4
Pb	ICP	ppm	2	bd	4	3	3		6	15	6	19	8	bd	6	2	3	bd
Bi	ICP	ppm	5	bd	bd	bd	bd		bd	bd	bd	bd	bd	bd	bd	bd	bd	bd
Th	INAA	ppm	0.2	8.7	8.0	8.3	8.2		11.0	29.2	21.2	23.7	12.0	16.0	20.8	11.0	13.0	19.0
U	INAA	ppm	0.2	14	5	5	5		8.1	12	21.4	13	7.1	8	14	6.5	12	241

Appendix Table 2 Element concentration raw data for bulk samples (continued a).

Grimsel Breccia samples (cont.)																**Host rock samples**				
6		8		10		14		16		17		18		26		46	48	72		
WC	ST	WC	ST	WC	ST	WC	ST	WC	ST	WC	ST	WC	ST	WC	ST	ST	ST	ST	ST	ST
109		118		92		53		143		34		113		126		11	7	7	7	7
bd		bd		bd		bd		bd		bd		bd		bd		11	bd	11	bd	5
188		123		188		157		275		453		487		142		264	112	223	181	*202*
0.67		0.3		0.45		1.04		0.64		2.36		0.69		0.11		2.13	2.4	2.59	2.51	2.51
0.74	0.86	0.31	0.34	0.45	0.49	1.2	1.1	0.72	0.74	2.6	2.8	0.77	0.75	–		2.47	2.94	3.02	3.02	3.02
0.09		0.02		0.07		0.06		0.46		0.3		0.11		0.06		0.28	0.18	0.18	0.17	0.17
4.37		3.04		4.02		5.15		3.4		7.58		4.12		4.07		7.19	6.52	6.93	6.76	6.76
2.83		2.24		2.77		3.28		1.72		3.03		2.31		3.64		3.09	2.89	3.14	2.73	2.73
0.1		0.06		0.08		0.1		0.29		1.14		0.38		0.1		0.13	0.12	0.3	0.28	0.28
2.6	3.5	1.8	2.1	2.4	2.8	2.2	2.7	5.1	4.9	4.7	4.3	3.3	3.1	3.5	3.6	4.9	4.4	4.4	4.8	4.6
0.11		0.03		0.1		0.05		0.16		0.21		0.14		0.09		0.09	0.07	0.08	0.08	0.08
8		6		9		5		35		18		13		14		13	7	8	7	7
3		6		4		4		54		9		6		3		176	240	174	165	165
<50	650	<50	450	<50	350	<50	360	100	310	<50	130	<50	300	<50	350	330	450	310	310	310
150		79		108		176		230		622		141		167		261	285	384	355	355
0.85		0.45		0.85		0.57		1.14		1.51		0.98		0.69		1.11	1.02	0.95	0.9	0.9
1.1	1.6	0.6	1	1.1	1.4	0.7	1	1.5	1.2	1.8	1.6	1	1.3	0.9	1.1	1.5	1.4	0.9	1	0.95
27		33		20		22		26		12		14		24		3	3	3	3	3
25	bd	29	bd	18	bd	18	bd	20	bd	bd	bd	14	bd	15	bd	bd	bd	bd	bd	bd
2		2		2		<1		20		4		2		2		4	5	4	3	3
1		1		1		5		7		<1		3		2		6	5	4	4	4
19		8		12		13		27		43		19		16		20	18	22	21	21
bd	bd	bd	bd	12		bd	bd	bd	bd	bd		13		bd		15	11	12	12	12
		22		14		bd		14		bd		7		157		bd	bd	bd	bd	bd
66	69	146	150	104	100	21	33	50	61	1.5	2.3	42	42	241	268	1.8	0.5	1.2	1	1.1
bd	bd	bd	bd	bd	bd	bd	bd	bd	bd	bd	bd	bd	bd	bd	bd	bd	bd	bd	bd	bd
<1	<1	<1	1.3	<1	<1	<1	<1	<2.1	<1	<1	<1	<1	<1	1.2	1	bd	bd	bd	0.6	0.6
320	310	250	250	320	320	260	280	190	190	240	240	260	240	390	400	260	190	190	210	200
42		35		33		46		58		162		82		21		67	68	73	71	71
11		8		9		14		7		19		9		16		29	25	30	30	30
7		5		6		bd		9		7		5		12		11	7	bd	bd	bd
7		5		8		9		<5		13		5		8		25	19	15	18	18
44		431		55		16		213		9		29		203		2	3	3	2	2
43	49	403	420	50	55	12	17	200	200	<2	3	22	25	190	200	5	6	5	3	4
bd		bd		bd		bd		bd		bd		bd		bd						
bd		bd		bd		bd		bd		bd		bd		bd		bd	bd	bd	bd	bd
bd	bd	bd	bd	bd	bd	bd	bd	bd	bd	bd	bd	bd	bd	bd	bd	bd	bd	bd	bd	
bd		bd		bd		bd		bd		bd		bd		bd		bd	bd	bd	bd	bd
7.4	7.2	22	21.7	5.3	5.6	1.7	2.3	19	20	0.3	0.4	5.3	5.5	14	16	0.2	0.1	0.1	0.1	0.1
22	19	15	16	25	22	4.7	6.3	10	10	4.5	3.6	12	11	19	18	3.4	2.2	2.2	3	2.6
301		144		266		254		214		596		359		146		639	459	516	504	504
400	310	150	170	400	290	290	320	220	310	700	710	570	350	220	190	590	390	450	490	470
10		6		7		11		14		41		28		11		27	35	38	38	38
11	14	6	7	7	8	12	12	16	15	46	47	31	31	11	12	28	41	43	43	43
21	33	<10	<10	12	<10	20	25	23	24	68	81	46	48	28	21	47	73	77	71	74
2.5	2.3	1.8	1.9	2	1.9	3.4	3.3	2.2	2.3	5.3	5.3	3.4	3.3	3.6	3.4	4.4	5.5	5.8	5.9	5.85
<2	<2	<2	<2	<2	<2	<2	<2	<2	<2	<2	<2	<2	<2	<2	<2	bd	bd	bd	bd	bd
<1	<1	<1	<1	<1	<1	<1	<1	<1	<1	<1	<1	<1	<1	<1	<1	0.9	1	0.9	1	0.95
<5	<5	<5	<5	<5	<5	<5	<5	<5	<5	<5	<5	<5	<5	<5	<5	4	3	4	4	4
<0.5	<0.5	0.6	<0.5	<0.5	0.6	<0.5	<0.5	<0.5	<0.5	<0.5	0.7	<0.5	<0.5	<0.5	<0.5	bd	bd	bd	bd	bd
3	3	<2	<2	3	2	<2	2	<2	<2	5	5	<2	3	<2	<2	5	5	4	5	4.5
1.4	<1.0	1.2	1.1	1.5	<1.0	2.1	2.2	<1.0	<1.0	2	2	<1.0	<1.0	1	<1.0	3	3.3	2.4	2.4	2.4
436	4	550	4	300	4	346	4	304	4	110	<2	170	5	421	5	3	3	2	2	2
bd		bd		bd		bd		bd		bd		bd		bd						
20		106		6		32		36		bd		30		bd						
12	<5	130	130	11	7	33	38	23	45	<5	<5	37	41	<5	<5	bd	bd	bd	bd	
21		46		15		bd		53		bd		28		48		bd	bd	bd	bd	bd
5		10.3		3.3		1.6		8.6		1.3		2.6		13.6		1.2	0.8	0.9	1	1
6		7		4		9		2		20		8		15		8	7	16	18	18
bd		bd		bd		bd		bd		bd		5		bd		bd	bd	bd	bd	bd
12.0	12.0	9.4	11.0	12.0	11.0	16.0	18.0	5.2	6.3	23.0	25.0	9.5	9.2	15.0	15.0	27.5	32.1	27.5	28.1	27.8
8.1	8.3	8.8	8.1	9.3	10	17	17	3.6	3.1	7.4	8.8	6	6.2	9.3	9.3	13	12	6.8	7	6.9

Appendix Table 2 Element concentration raw data for bulk samples (continued b).

				Host rock samples (cont.)						Recent thermal spring deposits						Soil samples	
		Sample Nr GR.		87	88	89			90	19	20	21	98	105	107.1	118	119
		Mill used(2)		ST	ST	ST	ST	ST	ST	WC	WC	WC	WC	WC	WC	ST	ST
El	Method		detection limit(1)														
Li	ICP	ppm	2	23	12	5	5	5	35	47		58		119	51	15	9
B	ICP	ppm	10	bd	12	bd	11	5	bd					11	18		
F	ISE	ppm	20	642	320	49	48	49	1706					294	167		
Na	ICP	%	0.01	2.4	3.55	2.47	2.45	2.45	2.25	1.17		1.66		0.39	0.57	2.2	2.6
Na	INAA	%	0.02	2.88	4.47	2.95	2.93	2.94	2.88	1.5	0.86	2.4		0.69	1.2	2.84	3.16
Mg	ICP	%	0.01	0.15	0.39	0.09	0.09	0.09	0.29	0.76		0.71		1.79	0.9	0.52	0.17
Al	ICP	%	0.01	5.49	7.64	6.48	6.43	6.43	6.52	4.27		7.21		5.72	3.5	6.09	6.76
K	ICP	%	0.01	2.41	2.12	2.78	2.57	2.57	2.13	1.53		2.07		1.93	1.58	1.73	1.95
Ca	ICP	%	0.01	0.12	0.29	0.11	0.11	0.11	0.48	6.09		5.06	1.5	0.84	3.59	1.12	0.57
Sc	INAA	ppm	0.2	2.5	5.1	4	3.5	3.75	5.2	6.4	5.1	7.8	6.5	8.6	6.3	8.9	6.3
Ti	ICP	%	0.01	0.02	0.17	0.02	0.02	0.02	0.16	0.14		0.16	0.38	0.29	0.14	0.18	0.17
V	ICP	ppm	2	6	20	5	5	5	18	20		26		47	26	35	33
Cr	ICP	ppm	2	120	178	138	155	155	124	21		25		9	3	216	160
Cr	INAA	ppm	20	230	360	260	270	265	240	53	<140	56		<110	270	430	360
Mn	ICP	ppm	5	48	304	179	430	430	308	>20000		11350	9705	4053	>20000	445	144
Fetot	ICP	%	0.01	0.43	1.59	0.75	0.92	0.92	1.39	7.68		1.81	5.1	6.93	>10	1.68	0.82
Fe	INAA	%	0.2	0.7	1.9	0.7	0.8	0.75	1.6	7.6	7	2.3		9.1	10	2.2	1.2
Co	ICP	ppm	1	2	6	2	2	2	5	9		8		18	11	7	5
Co	INAA	ppm	5	bd	bd	bd	bd	bd	bd	bd	bd	10		bd	bd	bd	bd
Ni	ICP	ppm	1	3	4	4	14	14	4	16		18		11	8	12	4
Cu	ICP	ppm	1	4	4	4	8	8	4	70		94		32	17	21	5
Zn	ICP	ppm	2	11	31	13	13	13	29	103		296	810	299	117	74	11
Ga	ICP	ppm	2	bd	12	bd	10	10	bd	bd		bd		25	bd	10	14
As	ICP	ppm	5	bd	bd	bd	bd	bd	bd	39		31		26	78	5	bd
As	INAA	ppm	0.5	3.8	2.4	4.3	4.5	4.4	5.6	57	2	17	29	32	56.4	10	1.4
Se	INAA	ppm	5	bd	bd	bd	bd	bd	bd	bd	<31	<10		<15	<11	bd	bd
Br	INAA	ppm	0.5	bd	bd	bd	bd	bd	bd	59	70	10		103	84	4.3	3
Rb	INAA	ppm	5	120	130	160	150	155	240	190	650	160	509	746	200	140	130
Sr	ICP	ppm	1	114	114	69	68	68	86	364		238		92	398	182	169
Y	ICP	ppm	5	18	20	25	24	24	18	28		23		29	51	27	18
Zr	ICP	ppm	5	14	5	18	17	17	bd	13		23		6	11	5	7
Nb	ICP	ppm	5	9	19	17	19	19	14	7		8		19	7	19	19
Mo	ICP	ppm	1	2	2	3	5	5	3	13		7		2	2	3	3
Mo	INAA	ppm	1	4	4	5	6	5.5	5	5	<10	5		14	<5	4	5
Pd°	FA-DCP	ppb	1														
Ag	ICP	ppm	2	bd	bd	bd	bd	bd	bd	bd		bd		bd	bd	bd	bd
Ag	INAA	ppm	0.5	bd	bd	3	bd	3	3	bd	<21	bd		<7	<5	bd	bd
Cd	ICP	ppm	1	bd	bd	bd	bd	bd	bd	bd		bd		bd	bd	bd	bd
Sb	INAA	ppm	0.1	0.4	0.1	0.4	0.4	0.4	0.6	27.7	12	20.2	31.1	17.3	30.2	0.7	0.2
Cs	INAA	ppm	0.5	1.6	1.9	0.5	1.3	0.9	6.5	54	322	22	258	492	86	6.4	5.5
Ba	ICP	ppm	5	589	619	664	661	661	682	391		494		502	440	543	739
Ba	INAA	ppm	50	540	500	570	610	590	610	460	820	810	820	270	310	500	700
La	ICP	ppm	5	20	41	23	22	22	34	23		23		18	34	44	43
La	INAA	ppm	2	22	49	25	24	24.5	42	26	17	36	25	20	33	56	51
Ce	INAA	ppm	5	39	88	51	52	51.5	77	63	44	61	65	<18	50	100	88
Sm	INAA	ppm	0.1	3.7	5.4	4.4	4.4	4.4	4.5	6.4	17	6.6	4.9	11.1	5.8	7.2	5.8
Eu	INAA	ppm	1	bd	bd	bd	bd	bd	bd	bd	<6	bd		<4	<3	–	–
Tb	INAA	ppm	0.5	0.7	0.9	1.1	0.8	0.95	0.7	1.2	1.7	<1		<0.5	0.9	1	0.8
Yb	INAA	ppm	2	3	3	4	5	4.5	3	<5	<5	<5		<4	<3	4	4
Lu	INAA	ppm	0.2	bd	bd	bd	bd	bd	bd	<0.5	<1.2	<0.5		<0.7	<0.4	bd	bd
Hf	INAA	ppm	1	3	5	3	5	4	5	<2	<9	<2		<5	8	8	9
Ta	INAA	ppm	0.5	1.4	1.7	2.1	1.9	2	1.7	<1.0	3.1	1.4	2.3	1.6	bd	1.9	2.2
W	INAA	ppm	1	1	3	2	2	2	2	59	<13	27		13	38	3	2
Pt	FA-DCP	ppb	5														
Au	FA-DCP	ppb	1														
Au	INAA	ppb	2	bd	bd	bd	4	4	bd	130	490	68	227	430	140	16	bd
Hg	AA	ppb	10	bd	bd	bd	bd	bd	bd	316		71		836	305	172	16
Tl	AA	ppm	0.1	0.7	0.6	1.2	1.1	1.1	1.5	2.6		3.3		5.7	3.1	0.6	0.6
Pb	ICP	ppm	2	6	bd	6	6	6	7	204		61		151	272	66	17
Bi	ICP	ppm	5	bd	bd	bd	bd	bd	bd	14		bd		bd	bd	bd	bd
Th	INAA	ppm	0.2	15.0	18.0	20.5	20.6	20.6	24.7	22.0	31.0	28.0	34.4	47.7	24.5	22.7	12.0
U	INAA	ppm	0.2	3.8	6.4	9	8.8	8.9	7.9	42	93.7	94.2	114	110	42.1	9	4.9

Appendix Table 3 Element concentration raw data (INAA) for chip samples.

		GRIMSEL BRECCIA: INDIVIDUAL CLASTS														
GR sample Nr		8								16			22		27	28
Subsample		8A	8B	8C	8D	8E	8F	8G	8H	16A	16B	16C	22B	22C	27.1B	28
El	Unit															
Na	%	0.29	0.32	0.18	0.31	0.41	0.27	0.31	0.25	0.55	0.09	0.28	0.46	0.56	0.46	0.36
Sc	ppm	2.6	1.5	1.6	1.7	1.5	1.3	1.7	2.2	9.5	5.0	3.9	2.0	2.7	4.6	2.4
Fe	%	0.56	0.42	0.56	0.29	0.33	0.32	0.48	0.58	1.95	1.03	0.84	0.74	0.71	1.14	0.81
Co	ppm	2.7	0.8	0.6	0.6	1.1	<0.19	3.8	<0.32	10.4	5.5	3.9	5.5	3.9	5.3	2.1
As	ppm	91.2	43.2	197	21.6	29.1	7.96	97.4	82	27.6	15.6	38.4	85.2	121	292	408
Se	ppm	<1.4	<1.3	<1.7	<1.2	<1	<0.9	<1.1	<1.5	<1.8	<0.9	<1.3	<1.5	<1.4	<1.7	<2
Rb	ppm	309	290	239	269	268	325	262	288	224	122	127	308	285	243	352
Mo	ppm	502	236	691	162	115	32.1	417	334	135	63.3	110	500	464	307	2630
Sb	ppm	20.5	14.8	22.2	8.88	21.3	3.98	18	14.3	12.5	6.69	10.8	16.7	24.8	9.72	23.2
Cs	ppm	26.2	17.8	16.6	18.1	17.1	11	17	28	13.4	16.7	14	20.8	23.5	19.7	13.5
Ba	ppm	171	128	94	180	208	189	156	115	307	126	86	211	242	199	767
La	ppm	8.2	4.2	5.5	6.9	7.1	4.6	8.6	7.5	18.0	4.1	7.4	8.5	12.5	17.0	19.7
Ce	ppm	19.5	9.4	12.5	14.4	15.8	10.3	19.2	19.8	35.0	8.0	14.4	19.7	26.7	33.6	38.1
Sm	ppm	2.2	1.2	1.4	1.6	1.6	1.3	1.9	3.3	3.0	0.8	1.3	2.3	2.9	2.7	3.2
Yb	ppm	1.58	1.19	0.9	1.25	1.21	1.11	1.39	2.44	1.51	0.56	0.64	1.98	1.97	1.57	1.94
Ta	ppm	0.82	0.63	0.3	0.69	0.72	1.03	0.86	1.12	<0.35	0.14	0.29	0.89	0.93	0.37	1.05
W	ppm	1.39	0.84	0.93	1.32	0.88	0.57	1.2	1.37	3.89	4.56	0.22	1.5	2.11	3.48	0.84
Au	ppb	55	15	134	17	36	3	42	66	18	8	37	39	40	217	168
Th	ppm	11.5	9.1	6.8	9.0	8.3	13.3	10.1	13.1	4.3	0.8	2.2	11.0	12.9	6.3	11.8
U	ppm	7.6	6.6	6.9	4.4	4.3	5.9	7.0	10.9	1.7	0.9	2.9	10.4	10.6	5.4	8.1
mass (g)		2.36	1.34	0.44	0.64	5.13	0.76	4.16	1.77	1.71	0.86	0.48	1.75	2.90	0.58	2.32

Appendix Table 3 Element concentration raw data (INAA) for chip samples (continued a).

		GRIMSEL BRECCIA: INDIVIDUAL CLASTS (continued)																
		34				36	52	53	61		84			102		135		
		34re	34B	34C	34.2	36	52	53re	61afk	61bfk	84green	84mix	84red	102.3g	102.3fk	135a	135a*	135b	135d
Na	%	0.38	0.26	1.22	0.38	0.13	0.62	0.66	0.38	0.51	0.02	0.80	0.06	0.56	0.11	1.38	1.51	1.08	0.73
Sc	ppm	3.3	4.1	2.4	3.0	2.1	1.7	2.2	6.7	10.0	0.3	2.1	1.2	5.4	5.0	2.9	3.0	2.9	3.7
Fe	%	0.79	0.94	0.48	0.67	0.71	0.8	0.52	2	2.7	1.5	1.2	1.1	1.4	1.2	0.46	0.48	0.56	2.22
Co	ppm	7.9	3.0	2.0	4.8	<5	<10	<5	11.0	14.0	<5	<5	<10	5.5	5.1	<0.28	<0.24	<0.36	4.2
As	ppm	147	33.3	32.1	176	7	609	121	458	241	133	183	188	207	135	4.82	6.71	7.41	784
Se	ppm	<5	<2.3	<1.6	<2.2	<5	<10	<5	<5	<5	<5	<5	<10	<5	<5	<1.4	<1.2	<1.9	<3.8
Rb	ppm	400	257	267	358	370	270	300	250	330	513	522	370	240	190	375	415	381	252
Mo	ppm	1170	52.4	117	934	16	2870	180	987	475	<8.1	<68	<79	209	152	<3.4	<4	<4.5	479
Sb	ppm	30.7	5.21	4.7	52.4	1.3	22.4	6.8	18.7	12.5	4.1	8.2	13	18.6	16.4	0.705	0.486	0.422	7.74
Cs	ppm	52.3	15.1	9.48	24.3	20	7.1	13	44	50	179	75	49	18	20	39.5	41.3	31.4	30.2
Ba	ppm	270	313	253	134	310	410	240	170	130	<150	<980	<1300	430	290	269	321	252	256
La	ppm	10.0	7.4	7.2	10.7	14.0	21.0	13.0	10.0	13.0	8.2	15.0	6.6	23.0	10.0	18.0	18.4	14.3	16.7
Ce	ppm	20.0	18.8	22.5	25.5	27.0	43.0	28.0	25.0	35.0	17.0	40.0	25.0	50.0	21.0	33.7	33.9	28.4	35.6
Sm	ppm	1.5	3.5	6.3	2.7	1.7	2.9	2.1	2.0	2.8	1.4	0.1	<2.6	3.1	1.4	3.8	4.5	3.6	3.1
Yb	ppm	1.7	1.92	4.82	2.11	1.4	<2	2.2	1.4	1.8	<1	2.3	3.2	1.4	<1	3.22	3.69	3.98	2.95
Ta	ppm	1	1.13	1.59	1.36	0.63	1.4	1.2	<0.5	0.76	<0.5	1.2	<1	0.79	<0.5	2.35	2.5	3.47	1.68
W	ppm	3.3	<2.3	0.45	1.94	0.5	1	1.8	3.9	6.5	0.5	1.9	2.4	2.9	2.7	0.62	1.31	1.71	2.14
Au	ppb	40	7	10	17	1	370	22	94	32	361	671	1100	14	14	1	1	1	3410
Th	ppm	12.0	17.8	12.7	15.2	9.0	11.0	13.0	3.1	4.4	0.1	11.0	7.5	6.5	2.0	20.2	18.8	24.1	23.1
U	ppm	11.0	14.8	8.9	15.9	4.3	6.3	6.8	2.0	1.9	26.4	188.0	255.0	1.9	0.8	11.9	13.6	15.2	18.1
mass (g)		1.19	0.17	1.72	1.59	1.63	0.63	1.82	2.64	1.40	1.09	1.96	0.52	4.02	2.26	2.86	3.25	1.02	0.55

Appendix Table 3 Element concentration raw data (INAA) for chip samples (continued b).

		GRIMSEL BRECCIA, U-RICH				GRIMSEL BRECCIA: SEDIMENTS, CHERTS											
		1		138		2	3	7		22	27	34	41	115		114	127
		1	1ore	138		2	3	7A	7B	22A	27.1A	34A	41	115		114gre	127b
Na	%	1.20	0.21	<4.2	Na	0.37	0.32	0.24	0.44	0.07	0.34	0.10	0.25	0.57	Na	0.06	1.53
Sc	ppm	3.4	1.5	2.1	Sc	3.9	4.0	4.0	3.9	2.8	4.2	3.9	3.1	1.8	Sc	0.5	2.5
Fe	%	1.5	2.2	3.65	Fe	1.21	1.26	1.73	1.78	0.56	1.17	1.08	1.00	1.4	Fe	0.62	0.52
Co	ppm	<5	<25	19.2	Co	2.1	1.4	6.3	4.7	1.5	5.3	28.2	<5	<5	Co	<5	0.7
As	ppm	1080	1910	2610	As	39.8	30.4	936	972	68.1	191	253	216	1320	As	17	1.74
Se	ppm	5.8	22	<4.5	Se	<1.4	<1.8	<6.1	<5.3	<1.9	<1.9	<1.9	<5	<5	Se	<5	<1.5
Rb	ppm	350	500	634	Rb	259	257	187	184	249	188	113	220	280	Rb	140	298
Mo	ppm	<320	<870	<2200	Mo	218	870	1590	1560	840	508	2160	1130	4610	Mo	<1	<1.9
Sb	ppm	88.6	228	266	Sb	14.7	72.9	131	106	103	11.3	38.6	189	36.7	Sb	10.7	0.904
Cs	ppm	7.8	18	28	Cs	21.3	27	17	15.9	30	20.6	17.4	25	8.9	Cs	49	12.4
Ba	ppm	<7800	<15000	<54000	Ba	407	388	<130	<130	122	108	130	330	410	Ba	<50	339
La	ppm	<26	<91	<1600	La	21.0	17.4	7.1	7.9	5.2	9.2	4.7	13.0	25.0	La	7.7	18.5
Ce	ppm	<160	<370	<1100	Ce	40.4	34.3	19.2	20.6	12.2	18.7	10.6	23.0	53.0	Ce	12.0	36.0
Sm	ppm	<11	<22	<75	Sm	3.0	2.6	2.8	3.0	1.6	1.5	2.0	1.9	3.6	Sm	1.2	3.1
Yb	ppm	3.3	<5	7.22	Yb	1.52	1.44	2.78	2.78	1.35	1.17	1.38	1.20	1.9	Yb	<1	2.34
Ta	ppm	1.2	<2.5	<0.49	Ta	1.22	0.98	0.76	<0.36	1.12	<0.44	0.39	<0.5	1.1	Ta	<0.5	1.76
W	ppm	10	17	<873	W	2.35	2.71	<0.64	<0.5	1.96	2.77	<1.3	1.40	<1	W	<1	0.9
Au	ppb	91	320	170	Au	33	130	233	239	19	278	167	293	742	Au	59	<1.7
Th	ppm	41.4	25.0	31.6	Th	9.2	7.6	10.7	13.9	9.5	4.2	2.1	5.9	11.0	Th	1.6	19.4
U	ppm	922	2310	8360	U	3.5	2.4	21.7	22.1	4.5	11.8	3.1	<3	6.7	U	4.8	6.4
mass (g)		1.52	0.12	1.50	mass (g)	3.17	3.04	1.70	2.36	0.62	1.48	0.48	2.09	0.83	mass (g)	1.14	3.00

Appendix Table 3 Element concentration raw data (INAA) for chip samples (continued c).

		GRIMSEL BRECCIA: CELADONITE-RICH											MISC SAMPLES			
		129			130			131				132		7	34	139
		127e	129e	129f	130a	130b	130c	131f	131g	131d	131e	132c		7C	34D	
Na	%	1.10	0.68	0.64	0.08	0.66	0.70	0.24	0.84	1.51	1.61	0.05	Na	2.52	1.10	1.15
Sc	ppm	3.5	2.0	3.5	1.6	3.3	5.3	2.0	4.0	4.9	2.7	1.3	Sc	2.8	1.3	10.2
Fe	%	0.58	0.49	1.02	2.7	0.32	1.44	1.99	0.73	0.83	0.52	1.73	Fe	0.41	0.3	3.98
Co	ppm	0.4	0.6	0.9	25.4	0.6	1.9	6.6	1.7	0.8	0.3	2.0	Co	<0.15	0.9	19.4
As	ppm	10.3	7.64	54.3	140	53	38.1	79.2	34.5	3.84	6.74	68.4	As	16.7	15.9	12.7
Se	ppm	<1.3	<0.8	<0.9	<7.8	<1.9	<1.5	<2.5	<3.2	<1.4	<0.6	<1.1	Se	<1.3	<1.6	<2.8
Rb	ppm	323	173	184	174	561	259	260	190	264	190	209	Rb	207	147	240
Mo	ppm	<4.1	13.5	410	95	<7	171	<5.7	<4.8	<4	<2.8	<5.8	Mo	<6.5	23.4	<18
Sb	ppm	2.06	2.71	3.64	10.3	2.77	2.52	7.61	4.56	1.12	1.6	12.5	Sb	0.886	2.19	0.914
Cs	ppm	15	18.9	18.3	59	15	13.9	73.5	30.4	18.6	11.5	32	Cs	0.75	4.22	49.5
Ba	ppm	383	211	189	<100	1140	323	61	122	366	243	<92	Ba	174	110	840
La	ppm	17.5	13.0	13.1	1.9	19.6	24.1	16.6	30.2	30.5	18.5	23.1	La	6.4	7.0	25.5
Ce	ppm	35.6	25.9	26.4	4.7	45.9	49.8	40.5	63.6	61.4	36.8	47.4	Ce	15.7	15.0	130.0
Sm	ppm	3.3	2.8	2.3	<0.19	5.6	5.4	3.3	5.8	5.7	3.4	4.7	Sm	3.4	1.7	6.6
Yb	ppm	3.77	2.13	2.91	0.54	4.07	4.66	2.89	4.31	5.13	2.81	1.5	Yb	5.79	1.6	3.1
Ta	ppm	2.52	1.37	1.24	<0.82	2.96	1.29	0.78	2.39	2.72	2.31	<0.14	Ta	4.66	0.92	1.42
W	ppm	1.27	0.53	1.33	<4	1.48	1.23	2.6	1.57	0.72	0.81	14.9	W	<0.55	<0.61	4.44
Au	ppb	15	9	208	40	<2.2	83	23	5	7	4	<1.5	Au	6	10	9
Th	ppm	17.5	11.7	16.3	6.4	26.3	16.0	8.3	23.7	27.4	15.6	2.7	Th	19.4	12.0	64.6
U	ppm	14.6	8.5	12.2	19.9	16.5	11.3	19.4	15.6	14.4	10.1	18.5	U	16.5	5.8	46.7
mass (g)		4.23	7.23	7.27	0.03	1.40	2.19	0.75	0.51	3.74	12.05	4.00	mass (g)	4.29	0.92	0.88